

NUMERICAL OPTIMISATION OF THE GATING SYSTEM OF A TITANIUM ALLOY INLET VALVE CASTING

JECOIS FOURIE

**Dissertation submitted in fulfilment of the requirements for the degree
Master of Technology: Mechanical Engineering
in the Faculty of Engineering
at the Cape Peninsula University of Technology**

Supervisor: Dr N Mahomed

Co-supervisor: Dr J Lelito

September 2014

DECLARATION

This dissertation is part of a double degree programme between the Faculty of Engineering of Cape Peninsula University of Technology (South Africa) and the Faculty of Foundry Engineering of AGH University of Science and Technology (Poland).

As part of the programme, the student completed the following courses at Cape Peninsula University of Technology:

COURSEWORK: STL500S: Continuum Mechanics and Intro to Finite Element Analysis MTD500S: Metallurgical Thermodynamics
COMPUTER AIDED DESIGN: Introduction to CATIA. One-week training programme at the Product Lifecycle Management Competency Centre, CPUT.
PATTERN MAKING IN FOUNDRY TECHNOLOGY: Principles of additive manufacturing and rapid prototyping. Rapid Pattern-Making of wax models for sand and investment casting. One-week programme conducted at the RPD Laboratory, University of Stellenbosch.
FOUNDRY TECHNOLOGY: SAND CASTING: Principles of Sandcasting. One-week internship programme conducted at Atlantis Foundries.
FOUNDRY TECHNOLOGY: INVESTMENT CASTING: Physical Aspects of Castings (Mould, Production, Materials, Solidification of Metals); Wax room process review (Wax room operations, Materials, Production work); Ceramic Shell room review (Shell room operations, Materials, Production work); Melting and casting review (Ceramic mould preparation, Ferrous and non-ferrous melting, Spectrographic analysis and casting). One-week programme conducted at the CASTCO Foundry.
SIMULATION OF CASTING PROCESSES: Introductory course on the use of MAGMASOFT: Process Modelling; Mesh Generation; Process Simulation.
Eight-week Product Design and Simulation project using CATIA and MAGMASOFT.

As part of the programme, the student completed the following courses at AGH University of Science and Technology:

Coursework:	ECTS
Mathematics for Engineers	3
Thermodynamics of Alloys	3
Theory of Foundry Processes	3
Physical Chemistry of Metallurgical and Foundry Processes	3
High Quality Iron Alloys	2
Nonferrous Alloys for Special Applications	2
Metal Matrix Composites	2

Metal Forming Products	3
Powder Metallurgy Products	2
Designing of CAMD Products	2
Finite Difference Methods	3
Applying CAD Systems for Design Casting Technology	2
Foreign Language (special)	3
Theory of Elasticity and Plasticity	3
Iron Alloy Castings	2
Nonferrous Alloy Castings	2
Numerical Simulation and Experimental Methods for Mechanical Characterisation of Solids	4
Computer Networks and Clusters	2
Applying Computer Methods to Optimise a Cast Strength	2
Object Oriented Programming and Database Programming	2
Design and Application of Advanced Engineering Materials	2
Multi-scale Modelling	2
Precision Casting Technology	2
Computer Aided Tooling Manufacturing for Foundry Engineering	2
Elective Course I: Casting Technology Design	1
Elective Course I: Developing Quality of the Surface Layer of Castings	1
Metrology of Foundry Processes	1
Art Casting Technology	2
Selected Aspects of Corrosion in Cast Materials	2
Designing of Information Systems for Production Management in Foundries	1
Numerical Simulation and FEM	3
Seminar	1
Project	10

I, Jecois Fourie, declare that the contents of this dissertation represent my own unaided work, and that the dissertation has not previously been submitted for academic examination towards any qualification outside of the double degree programme. Furthermore, it represents my own opinions and not necessarily those of the Cape Peninsula University of Technology.

Signed

Date

ABSTRACT

The research described in this dissertation investigates the feasibility of casting inlet valves for an internal combustion engine using Ti6Al4V alloy. The engine valves operate in an extreme environment under high thermal cycles – this requires a material that can withstand such exposures. Ti6Al4V is the most common titanium alloy with high temperature creep and fatigue resistant behaviour, however, it is not all positive. Ti6Al4V alloy also yields many difficulties with respect to processing especially when the material is cast. It is therefore important to gain a thorough understanding of the pouring and solidification characteristics of this material.

The main focus of this work was to investigate and optimise feeding and geometrical parameters to produce valves that are free from defects, especially porosity.

An in depth analyses of the parameters that influenced the casting quality was performed, and it was found that casting orientation, inlet feeder geometry, initial and boundary conditions all played a vital role in the final results. These parameters were individually investigated by performing detailed numerical simulations using leading simulation software for each of these cases. For each case, a minimum of ten simulations was performed to accurately determine the effect of the alteration on casting soundness and quality. Furthermore, the relationships (if any) were observed and used in subsequent optimised simulations of an entire investment casting tree.

The change of geometric orientation and inlet feeder diameter and angle showed distinct relationships with occurrence of porosity. On the other hand, alteration in the pouring parameters, such as temperature and time, had negligible effect on occurrence or position of porosity in the valve.

It was found that investigating individual parameters of simple geometry and then utilising these best-fit results in complex geometry yielded beneficial results that would otherwise not be attainable.

ACKNOWLEDGEMENTS

I wish to thank:

- Dr Janusz Lelito – For his guidance and support whilst writing my dissertation. I would also like to thank him for his constant encouragement and kind words that helped to keep me motivated. His door was always open for questions.
- Dr. Nawaz Mahomed – For his supervisory role and for enabling this opportunity to further my studies internationally.
- Dr Jan Wertz – For his expert knowledge in casting technologies and providing ideas towards improving design and motivating the outcomes and results.
- Dr Piotr Kustra – For his knowledge and assistance surrounding FEM and his friendly and helpful demeanour. His door was always open and he always made time for questions. Also, for his ability to guide me without giving me the answer.
- Dr Pawel Zak – I would like to thank him for his friendly, helpful and highly knowledgeable background with numerical modelling. Information obtained from his lectures greatly assisted in the overall understanding of numerical analysis.
- Marek and Lukasz at Kom-odlew, Poland – For their friendly and helpful demeanour towards assisting me with the set-up of numerical simulations.

The financial assistance of the Department of Science and Technology, under its Technology Localisation Plan, towards this research is acknowledged. Opinions expressed in this thesis and the conclusions arrived at, are those of the author, and are not necessarily to be attributed to the Department of Science and Technology.

DEDICATION

I would like to dedicate my thesis to my loving parents,

Jean and Elma Fourie

Table Of Contents

Nomenclature	x
Glossary	xi
1. Introduction.....	1
1.1 Background	1
1.2 Problem statement	1
1.3 Facilities	2
1.4 History and extraction of titanium.....	3
1.5 Use of titanium in engine components	3
1.6 Titanium Alloy Phases	5
1.7 Manufacturing of Titanium Alloys	6
1.8 Properties of Titanium Alloy	7
1.8.1 Castability of titanium	7
1.8.2 Investment casting	8
1.8.3 Pattern preparation	11
1.8.4 Casting Porosity.....	11
1.9 Hot Isostatic Pressing (HIP).....	12
1.10 Gating system design	13
1.11 Research Objectives	14
2. Numerical method for the analysis of a heat transfer process.....	15
2.1 Introduction.....	15
2.2 The Mathematical Model	15
2.3 Thermo-physical parameters	19
2.4 Initial conditions.....	19
2.5 The Numerical Model.....	20
2.5.1 The Finite Difference Method	21
2.5.2 The Finite Element Method (Galerkin).....	24

3. Numerical Investigation of the investment casting process	26
3.1 The Geometric Model	26
3.2 Investment casting gating system design calculations	26
3.2.1 Volume of the casting.....	27
3.2.2 Mass of component.....	27
3.2.3 Modulus of the component	27
3.2.4 Feeder and downsprue modulus	28
3.2.5 Nominal downsprue diameter	29
3.2.6 Optimal flow velocity.....	30
3.2.7 Minimum safe diameter through which the material can flow.....	30
3.3 Numerical Analysis:	31
3.3.1 Analysis for individual inlet geometry.....	32
3.3.1.1 Change of component orientation	32
3.3.1.2 Change of inlet length.....	36
3.3.1.3 Change of inlet diameter.....	38
3.3.1.4 Change of inlet feeder shape	43
3.3.1.5 Change of inlet angle.....	45
3.3.1.6 Addition of insulation and change of insulation diameter.....	47
3.3.1.7 Change of initial temperature.....	50
3.3.1.8 Change of pouring time	51
3.3.1.9 Change of mould temperature	53
4. Numerical Simulation of Casting Design.....	56
4.1 Introduction.....	56
4.2 Design of casting tree.....	56
4.3 Results	58
4.4 Conclusions.....	61

5. Conclusions and Future Work	62
5.1 Conclusions.....	62
5.2 Future work	63
List of Figures	64
List of Tables	66
References	67

NOMENCLATURE

V	Volume in cubic meters (m^3)
m	Mass in kilograms (kg)
M	Modulus of casting – volume per area (mm)
ρ	Density in kilograms per cubic meter (kg/m^3)
l	Length in meters (m)
g	Gravity constant in meters per second squared (m/s^2)
C_p	Specific heat capacity (J/kg.K)

GLOSSARY

AGH	Akademia Górniczo-Hutnicza University of Science and Technology, Kraków, Poland
BCC	Body Centred Cubic, an atomic arrangement
CPUT	Cape Peninsula University of Technology
CAD	Computer Aided Design
CFM	Control Volume Method, a numerical technique used for solving differential equations
EPA	Environment Protection Agency
FDM	Finite Difference Method (Euler method), a numerical technique for solving differential equations
FEM	Finite Element Method, a numerical technique used for solving differential equations
FEA	Finite Element Analysis
HCP	Hexagonal Closed Packed, an atomic arrangement
HIP	Hot Isostatic Pressing, a high pressure high temperature process used extensively in titanium alloys to produce defect free components
PDE	Partial Differential Equation
SEM	Scanning Electron Microscopy
WRM	Weighted Residual Method, a numerical technique used for solving differential equations

1. Introduction

1.1 Background

In recent years, the improvement of internal combustion engines has become a crucial factor in the development of motor vehicles. Major pressure from environmental protection agencies around the globe have pushed the development of lighter, more fuel efficient vehicles that produce less toxic substances, especially in built-up inner city areas where pollution is of great concern. Reduction of inertial masses inside the engine directly affects not only acceleration and improvement in vehicle performance characteristics, but also increases engine component durability and lifespan. By investigating lighter, stronger and tougher materials that can operate under increasingly higher pressures and working temperatures, future internal combustion engines will be more fuel efficient and be more likely to be used in conjunction with alternative propulsion methods rather than being replaced.

Investigation into manufacturing of light weight, high-strength titanium alloy components will yield beneficial results in the dynamics of the internal combustion engine with improved fuel efficiency and durability with reduced emissions. These components must withstand high pressures and working temperatures, and Ti-6Al-4V, an alpha-beta alloy previously used for its high temperature properties and heat treatment possibilities, fall into the required specifications due to its advantageous properties.

1.2 Problem statement

High temperature titanium alloy presents a major opportunity for production of aerospace-grade components for the automotive industry, such as high temperature engine inlet valve components. Besides the drastic reduction of waste in forming near-net shaped components using precision casting technology, the effect on the microstructure of the material by excessive machining is also avoided.

There are common issues with as cast components and specifically titanium-based alloys that must be addressed at this point. One such major issue is the fact that titanium-based alloys have an affinity for oxygen, which leads to defects such as porosity as well as extensive shrinkage porosity.

To address these issues, it is necessary to more closely investigate the investment casting process involving such alloys. Part of this investigation includes the design and optimisation of the feeding (or gating) system, especially in cases that involve the simultaneous feeding of multi-cavity moulds.

This requires:

- (a) Understanding the mechanics of casting Ti-6Al-4V in an investment casting process.
- (b) Understanding the influence of temperature dependent parameters on the component's final properties.
- (c) Investigation into the feeder parameters and understanding the influence of inlet feeder and casting geometry on the final properties of the component.

As an application, the design of a feeding system for a multi-cavity investment casting mould for the production of Ti-6Al-4V engine inlet valve components will be considered. To make this process viable for industry, an investment cast tree containing as much as 50 valves that must be cast simultaneously will be considered in the study.

1.3 Facilities

The Faculty of Foundry Engineering at AGH University of Science and Technology in Poland was established in 1951 and specialises in Foundry Technology and Foundry Machinery. The Faculty educates specialists in the field of foundry technology and is the only faculty of this kind and scope of education operating within higher education system in Europe. This study made use of computer facilities at the AGH.

The company Kom-Odlew Computer Engineering Systems Sp. was founded in 1995. The initial profile of activity associated with the optimisation of casting technology using computer simulation of casting was subsequently extended to the overall problem of computer-aided design (CAD), computer aided manufacturing (CAM) and computer aided engineering (CAE), through cooperation in this area with the world leaders in the field of metal casting such as Magmasoft.

Through the assistance of onsite personnel at Kom-Odlew, numerical simulations could be undertaken and issues for subsequent investigation addressed. Bi-weekly meetings were also held at the premises to obtain relevant information.

1.4 History and extraction of titanium

The earliest known discovery of titanium ore was by an English mineralogist who investigated magnetic black sand in Cornwall in 1791. He called the sand Menachanite, after the name of the city where it was found. A few years later in 1794, Klaproth found a similar black 'sand' in rutile and named it titanium after the mythological Titans [107]. It took another two centuries to find a method to extract pure titanium in a commercially viable way [53].

Titanium is the ninth most abundant element in the earth's crust and the fourth most abundant metallic element [29, 30, 65, 76, 79, 101], and it appears in the crust as rutile and ilmenite [79].

The most popular method currently for extracting pure titanium from rutile and ilmenite is called the Kroll process, but other competing processes are also used with similar initial steps. The first step of the process involves extracting titanium slag through an enrichment process. Step two involves producing titanium tetrachloride ($TiCl_4$) through a chlorination process. Here the chloride is added to titanium and heated to $1000^\circ C$ to produce a gas, $TiCl_4$. From this, the $TiCl_4$ is reduced to pure titanium by cooling it back to a liquid of $600^\circ C$. Magnesium is added and the mix is held at $600^\circ C$ for four days.

The pure titanium is now in the form of sponge that must be processed through casting or forging processes [29]. The complexity of the aforementioned process gives rise to the high cost of titanium metal.

1.5 Use of titanium in engine components

Intake and exhaust valves in internal combustion engines are required to control the flow of gasses into and out of the combustion chamber by opening and closing through the valve train as indicated in Figure 1.1. The intake valve is responsible for inlet of cooler air and the outlet valve for the removal of hot exhaust gasses [55]. These valves are required to work under high thermal and cyclic stress conditions and must function without fail.

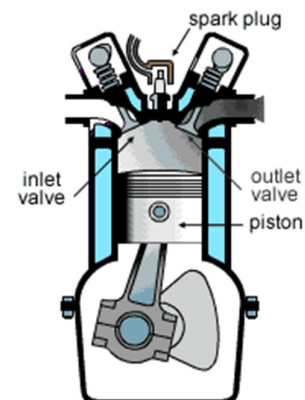


Figure 1.1 - Combustion chamber of an internal combustion engine [33].

Any failure, be it fatigue, high temperature creep or surface corrosion, could lead to ultimate failure of the component and

subsequent engine failure. Although the entire structure of the valve is important, three main areas are crucial: The seat surface must always be without defect as this surface prevents gasses from leaking out of the high pressure combustion chamber. Fatigue failure could occur at the head of the valve which causes radial and transversal cracks due to mechanical bending stresses. These cracks could further propagate due to the corrosive high temperature environment and lead to valve failure. Any porosity, due to casting procedure, in the head and stem will lead to corrosion and valve failure. Furthermore, the stem and valve seat of the valve should be resistant to high temperature creep and fatigue. An elongation will lead to gasses escaping from the combustion chamber prior and during combustion. The keeper groove is subjected to tensile stresses and, due to the reduced section, stress concentrations. Although there are many modes of failure including wear, valve face recession, erosion, overheating, carbon deposits, the most common mode of failure is fatigue [56, 103].

A standard Otto cycle and Diesel internal combustion engine presents a wide variety of power outputs and consequently a variety of temperature and pressure values. A maximum value for intake temperature has been recorded as 550°C. Maximum localised stresses in the order of 15MPa, in addition to these high temperatures, justifies the use of special high temperature creep and fatigue resistant materials [56-57, 103].

Table 1.1 shows the most widely used titanium alloy used in industry, Ti-6Al-4V. This makes this alloy of great importance for this study. The following section describes the effects of the alloying elements listed in Table 1.1 below, on phases present at room temperature and therefore subsequent microstructural and material properties.

Table 1.1 - Composition of Ti-6Al-4V [31].

Estimated relative use of castings	Nominal composition, wt%													Special Properties
	O	N	C	H	Al	Fe	V	Cr	Sn	Mo	Nb	Zr	Si	
85%	0.18	0.015	0.04	0.006	6	0.13	4	General Purpose

1.6 Titanium Alloy Phases

Commercially pure titanium promotes an allotropic phase with slow transformation at 883°C as illustrated in Figure 1.2. Below this temperature, the structure is hexagonal closed packed (hcp). Alternatively referred to as α -phase. Phase above aforementioned temperature is body-centred cubic (bcc), alternatively referred to as β -phase.

The phase temperatures and crystallographic orientations can be altered by addition of alloying elements. In the case of Ti-6Al-4V, the α - β phase transformation occurs at 980 °C illustrating the effect of alloying elements on transformation temperature.

Titanium alloys can therefore be classified as either α -, near- α , α/β or β phase and they are differentiated through their chemical composition, the weight percentage of alloying elements and resulting microstructure at room temperature [8, 36, 89, 42].

Alpha alloys have superior creep resistance to that of β alloys [79]. The principal alloying element in alpha alloys is aluminium in the order of 6wt%. Aluminium is also an α -phase stabiliser reducing the α/β transition temperature. When these alpha alloys are alloyed with β -alloying elements, they are classified as α/β -phase alloys. These α/β -phase alloys are processed in the upper α/β or β fields to achieve a variety of microstructures depending on the mechanical and resistance

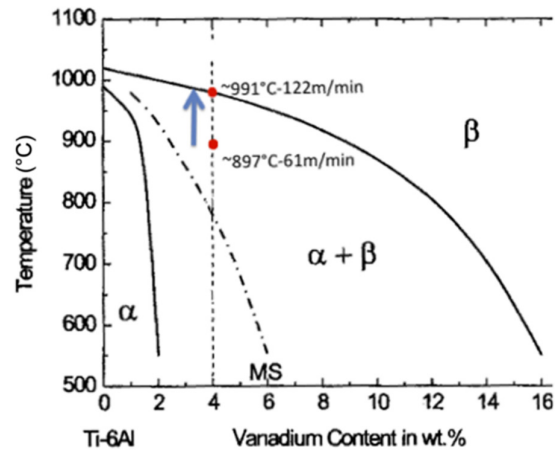


Figure 1.2 - Ti6Al4V phase diagram [100].

properties that are required. However, they all have the basic structure of platelets of beta lamellae arranged in colonies inside the grain. The alloy to be investigated in this study is an α/β -phase alloy that exhibit enhanced high temperature properties and creep resistance due to the aforementioned microstructure.

It is evident that Ti6Al4V is a complex alloy with a wide variety of possible properties, each specific to the mechanical, fatigue and corrosive properties required. The casting process, specifically the method and rate of solidification, greatly impacts possible phases that would be present at room temperature before the addition of post-processing heat treatment.

As mentioned above, this alloy is favourable for heat treatment procedures that improve the material's high temperature characteristics. Heat treatment and its effect on the mechanical properties of the alloy will, however, not be investigated in this study.

1.7 Manufacturing of Titanium Alloys

Unlike the more conventional metals such as iron, aluminium and bronze, for which processing routes have been well established, titanium can be seen as rather unconventional due to the highly controlled environments, alloying element additions and morphology possibilities, which makes it rather difficult to control.

Currently, the limiting factor for the mainstream usage of titanium alloys is their production cost, as discussed in Section 1.4. This causes customers to shy away from current titanium usage and rather opt for the “well known” rather than the “best new” approach. After all the processing parameters such as static and dynamic properties, chemical resistance, weight and specific density, casting complexity, mould composition and material cost have been taken into account, titanium alloys become rather profitable.

Titanium, although a very attractive metal because of its specific weight and corrosion resistance, has a strong affinity for reaction with oxygen, nitrogen and carbon. This affinity plays a major role when processing this material and attributes the high cost of titanium. According to Leyens and Peters [70], titanium's affinity for oxygen causes several defects. Such defects include embrittlement, increase in hardness and a reduction in fatigue life [75].

Titanium's high melting temperature range of 1600 to 1700 °C, and specifically that of Ti-6Al-4V with a liquidus temperature of 1688 °C, causes it be highly reactive in moulds. This reaction in common moulds cause a hard brittle α -case on the surface of titanium alloys. The α -case phase is stabilised by the interstitial oxygen and/or carbon that is absorbed during the breakdown of the mould. This α -case layer can cause crack initiation in severe cases. It is undesirable and must be removed from the casting [17].

1.8 Properties of Titanium Alloy

Ti-6Al-4V alloy yields excellent yield strength even at elevated temperatures [31]. The maximum working temperature for Ti-6Al-4V is 300-350°C [14, 62], but the elevated temperature can safely be raised to 450°C without excessive effects on the yield strength.

In the ($\alpha + \beta$) to β phase transformation temperature of 980°C, which is well below solidification temperature, the β dendritic structure transforms during solid state cooling to an $\alpha + \beta$ platelet structure typical for β processed wrought components. Properties such as creep resistance and crack propagations are superior to those of wrought components. Furthermore, the allotropic transformation of most titanium alloys allows the microstructure to be altered during post processing, adjustment of cooling rates and Hot Isostatic Pressing (HIP) [32, 82].

1.8.1 Castability of titanium

Castability has been described by many researchers. Baran [9] described castability as the “ability of an alloy to faithfully reproduce sharp detail and fine margins of the wax pattern”. Presswood [80] also stated, amongst others, that castability is the “ability of a molten metal to completely occupy the mould created by the elimination of a pattern”. Whatever the definition, it is clear that castability is a function of ability to fill the mould successfully and exactly replicate the removed wax pattern. Some factors that influence the castability of titanium are as follows:

- Gating design [22, 68, 73]
- Type of casting alloy [5, 25, 83]
- Casting temperature of metal alloy [15, 48]
- Mould temperature [1, 43]
- Mould size and space [52, 61]
- Chemical composition of mould material [19, 72, 95]
- Permeability of the investment mould wall [49, 87]
- Type of casting process [11, 97, 104]
- Specific gravity of the metal or alloy [78, 97, 102] and
- Position of the pattern in the mould [69, 74]

These and other factors mentioned above are addressed in the numerical investigations in this study.

1.8.2 Investment casting

Casting is a process whereby a molten metal is poured into a cavity of the desired final shape. After solidification, the metal assumes the shape of the mould cavity. Casting processes are employed under the following conditions [18]:

- The final component is too large to be manufactured in any other way.
- The final component is too complicated to be manufactured in any other way.
- The metal's ductility is too low to be formed by any other processes.
- Casting is the most economical process.

The term 'casting' is often associated with products that are inferior to wrought products, but this assumption is not true for titanium cast components, which are often superior due to the unique phase transformation properties [30, 34].

Koch *et al.* [58] suggested in their studies that investment casting of titanium is the method of choice for producing shapes with high dimensional accuracy and good surface finish. Donachie [30] added that titanium investment casting has been extensively used in aerospace industry due to the significant strength to weight ratios, but also due to production of precise components and near-net shapes requiring minimal machining and material loss. According to Taylor [98], technological advances in this field has made investment casting among the most versatile of all casting processes.

Casting of titanium yields its own set of difficulties. Firstly, titanium cannot be melted using conventional methods due to its high affinity to oxygen and hydrogen. Current melting techniques make use of electric-arc pressure/vacuum or centrifugal casting machines protecting the titanium from contamination under an argon or helium gas environment [79, 91].

Secondly, titanium reacts adversely with many currently utilised investment mould materials [10] which produces porosity and voids [19]. The materials chosen for the production of the ceramic investment shell is therefore very important especially with titanium alloy production. In ferrous metals, the investment medium is made up of zirconia, silica and alumina/silica, but due to titanium's aforementioned affinity for oxygen, this mould medium will produce castings of poor surface quality and porosity. Gas bubbles can be produced because of the reaction of the titanium with the shell, which in turn causes gas porosity [47].

To overcome this, studies by Syverud [93] suggested the use of gas permeable moulds to remove some of the gas build-up. Additionally, mould media such as zirconia must be employed. Phosphate-bonded mould materials contain increased amounts of zirconia oxide, but more recently, magnesium oxide and calcium oxide refractory materials have been employed [44, 49, 95].

Additionally, Jones and Yuan [54] found that the ceramic shell (mould) should have the following characteristics:

- Sufficient green and fired strength.
- High thermal shock resistance to prevent cracking once metal is poured.
- High chemical stability to prevent mould-metal interaction.
- Sufficient mould permeability to allow for the gasses to escape.
- Sufficient thermal conductivity to allow heat to be removed from the system and allow the casting to cool.
- Limited creep characteristics to provide a casting of close dimensional tolerances.

Thirdly, titanium has unusual flow characteristics in the molten state with poor thermal conductivity and rapid solidification [29, 53, 96]. Takahashi [95] suggested that the main reason for this is due to titanium's low density compare to other metals. To overcome the rapid solidification of titanium, the mould cavity must be filled rapidly [104].

Finally, if the temperature difference between the molten metal and the mould material is too high, costly miscasts can occur [21, 47, 97, 104].

Some methods can be employed to overcome the defects listed above by superheating the alloy, but due to titanium's poor thermal conductivity, it does not respond well to superheating processes [29].

The recommended mould temperatures for casting titanium varies from room up to 600°C [43, 97, 104]. If the walls of the mould are too cold, the walls will solidify first causing the walls to be impermeable, stopping the gasses from escaping. This would cause surface porosity resulting in poor surface quality. Also, to improve mould filling and mould filling time, it is highly recommended to design the gating system with the shortest path in mind [53].

Figure 1.3 illustrates the standard investment casting process that is gravity fed. Some aspects of the investment casting process with relevance to the investigation will be discussed in further sections, and the main concepts are listed below.

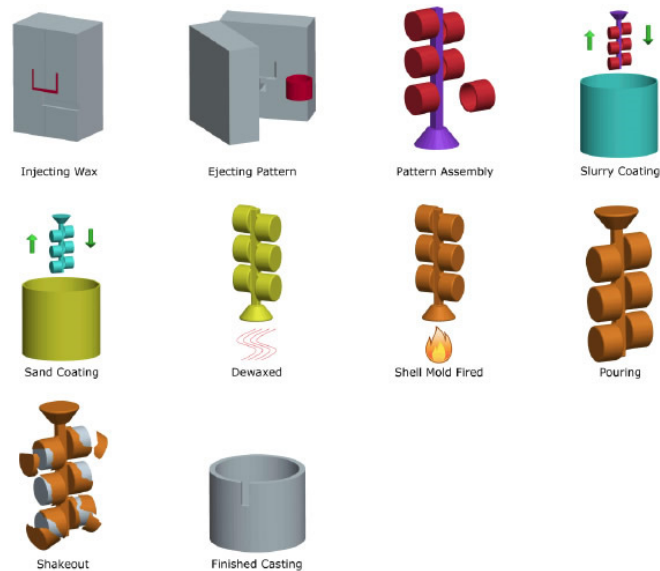


Figure 1.3 - Investment casting process under gravity [37].

To prepare the investment mould, a wax preform or pattern must be created. For this process, various methods are available. For single production processes, the wax pattern can be created using 3D printing techniques, carved out of wax if dimensional accuracy is not required, or alternatively (and most often utilised) injected into a steel die. The next step involves the assembly of the wax patterns onto a wax tree. The geometry and placement must be carefully calculated to allow for proper feeding. The completed wax tree is then covered in various layers of ceramic slurry. The thickness and grain sizes are dependent on the material being cast and the quality required. The ceramic coat is left to dry in ambient atmospheric conditions.

The ceramic shell is then dewaxed by placing it in an autoclave. The high heat and partial vacuum removes the wax pattern through a melting and draining process. Additional firing of the shell is required to remove all wax residue and harden the shell for the investment casting process.

The next stage involves the actual casting, or pouring. The pouring process can be completed in a variety of ways. Either through gravity feeding, which is the simplest and cheapest option, but requires careful planning with respect to geometry and material used. Additional pouring

methods include centrifugal casting and vacuum-assisted casting. These alternative processes are more costly and time consuming.

After pouring the part is removed from the shell and finished if required.

1.8.3 Pattern preparation

For the investment casting process, the pattern is made from wax, either organic or synthetic, although synthetic wax is most commonly used in industry today. This wax has a low melting point and has a high modulus of rigidity and low shrinkage. The pattern is produced in such a way that it has the exact geometry of the final cast component with additional dimensional allowances for the volumetric shrinkage of the wax upon solidification as well as to compensate for the shrinkage of the cast metal inside the mould [28].

According to investigations conducted by Craig and Eick et al. [28] the wax pattern must have the following properties:

- lowest thermal expansion coefficient,
- melting temperature should be as low as possible and as close to ambient temperature,
- resistant to breakage,
- a smooth surface after wax solidification to provide a smooth surface for casting,
- a low viscosity when melted to assist flow into thin sections of the mould,
- release easily from the mould after solidification,
- environmentally safe.

It is well known in industry that troublesome issues that arise for a ferrous caster is most often devastating to a titanium caster. It is therefore important when dealing with titanium alloys, such as the investigated alloy, that great care must be taken into choosing the correct wax. High ash content in the wax, for instance, can lead to excessive defects in casting often leading to castings being scrapped.

1.8.4 Casting Porosity

When solidification of an alloy inside an investment cast mould is not compensated for by additional feeding, porosity will occur [90, 99]. These porosities reduces the cross-sectional

area which adversely affects the mechanical properties. Also, these defect sites are potential crack initiation areas for failure [63].

In the case of titanium, the defects are generally limited to shrinkage porosity, but porosity due to gas, discussed in later section, also occurs. Donachie [29] stated that the porosity does not affect the tensile properties, but adversely affects the creep and fatigue strength of the alloy.

Some factors that contribute to the porosity in castings are shrinkage of the metal, gas removal, alloy composition, casting process, heating methods, temperature of mould, reactivity of mould with casting alloy, pattern and gating system design [11, 22, 64, 68].

According to Flemings [38], there are a number of resistances to heat flow from the molten metal to the surroundings that affect the solidification time and locale, which in turn are responsible for generation of hotspots and subsequent defects such as porosity. These resistances are as follows:

- The liquid metal
- The solidified metal
- The metal/mould interface
- The mould
- The surroundings of the mould

1.9 Hot Isostatic Pressing (HIP)

Titanium's affinity for oxygen and other elements such as nitrogen and hydrogen is also responsible for gas porosity, which negatively affects the final casting [20, 47, 93]. For this reason, and to reduce the risk of elemental contamination, titanium alloy castings are preferably produced under vacuum or under protective environment such as argon gas. These castings are inherently good, but defects such as shrinkage porosity and gas porosity still occur and, for this reason, it is common practice to apply HIP to the castings to remove such defects.

Polmear states that the static strength (maximum tensile and compressive strength under non-dynamic load conditions) of titanium castings are similar to those of wrought material with the same composition.

During the casting process, many defects can occur as previously mentioned in other sections. During the solidification, poor feeding causes shrinkage in core areas. In most cases, these defects cannot be eliminated through improvement of the feeding system, and the use of HIP becomes necessary. HIP is typically performed at 1000bar pressure in an inert atmosphere and at 900°C. At these temperatures and pressures, the material is free to creep without affecting the macroscopic dimensional stability.

1.10 Gating system design

Since the early 20th century, researchers have been interested in successful sprue design (the main cavity in a ceramic mould that is used to feed the casting with molten metal) to improve material properties. The entire system is often referred to as a casting tree.

Sprue design is one of the most crucial design considerations as improper design always leads to defects and miscasts [67, 99]. Shell [88] suggested that the metal must flow to all the extremities of the mould before solidification starts. Also, the metal must remain molten in areas that will solidify last to prevent hot spots and internal porosity [23, 99]. Brockhurst [15] added that porosity can be eliminated by proper sprue design.

To provide a successful sprue design, two important guidelines have to be taken into account. Firstly, the solidification should always be directional from the furthest part of the casting towards the feeding neck [17]. Secondly, the feeder must contain sufficient amount of liquid metal to account for the extreme shrinkage that occurs with titanium alloy castings.

According to Magnitskii [66], titanium alloys have a tendency to shrink up to 3.5% volume percent, or even higher according to Suzuki et al. [91]. If these casting guidelines are not carefully followed the, volumetric shrinkage will result in porosity favouring the last to solidify areas or hotspots. What is more troublesome is that the areas plagued with porosity are directly related to casting geometry and feeding and gating system design [81]. It is therefore important to look at optimising the feeding system by removing areas that could cause turbulence [90] as well as the initial geometry of the cast part to reduce such porosity.

1.11 Research Objectives

The main objective of the research is to study and compare the feeding characteristics of Ti-6Al-4V alloy with results obtained from numerical simulations. The objective will require the following to be completed successfully.

- **Design of the inlet valve schematic making use of design software DSS Solidworks™.** The initial design of the valve and inlet geometry will be visualised in Solidworks™ to be used in further investigations.
- **Investigation of feeding systems for casting of Ti-6Al-4V alloy by investment casting.** All the parameters that influence the quality of the final cast samples will be investigated individually. These parameters include design alterations to the sprue inlet position, orientation and shape. Also, initial and boundary conditions such as pouring and mould temperatures will be investigated. Each parameter will be investigated individually and results will be investigated. Further investigations into the results will be performed to determine relationships between parameters and alterations.
- **Gating and feeding system optimisation.** Data obtained from all numerical simulations will be investigated and optimised for a complete gating system. The best results for each investigated individual case are used as initial and boundary conditions for the complete casting. The results obtained will determine the validity of optimizing a complex design geometry by investigating the individual parameters that influences the final result and combining them together.

2. Numerical method for the analysis of a heat transfer process

2.1 Introduction

There are three steps to computational modelling. The first is to idealise the problem with a set of quantities that we, the user, would like to determine or measure. In some cases the problem is easily idealised and has a unique solution that can be analytically solved. In most real world processes, however, this idealisation is not guaranteed.

The second step is to model the process mathematically. This mathematical model is the set of governing equations that accurately represents the process. For example, the Navier-Stokes equations models the flow of the liquid melt and is an accurate representation of the actual process. Similarly, the Fourier-Kirschhoff equations can be used to model the heat conduction, convection and radiation processes.

The final step is to find the numerical solution to the process. The numerical solution is a set of PDEs that is solved over the entire solution space.

Usually in industry the design of components are an expensive and time consuming task and through the use of these numerical models, foundry men and engineers are able to effectively design optimal solutions for complex casting processes.

2.2 The Mathematical Model

Equation 1 is the Fourier-Kirchoff equation that relates to the flow of heat through and between materials and used as the base model for further numerical models.

$$C(T) \frac{\partial T}{\partial \tau} = [\lambda(T) \cdot \nabla^2 T] + q_V \quad (1)$$

where $C = \text{Volumetric Specific Heat (J/m}^3 \cdot \text{K)}$

$T = \text{Temperature (K)}$

$\lambda = \text{Thermal conductivity (W/m.K)}$

$\tau = \text{time (s)}$

and $q_V = L \cdot \frac{\partial f_s}{\partial \tau} \text{ (J/kg)}$

where $f_s = \frac{V_s}{V}$, and $f_s = f_s(x, y, z, t)$ and represented as a value from 0 to 1

$L = \text{Volumetric latent heat (J/kg)}$

$V_s = \text{Volume fraction solid in investigated zone}$

$V = \text{Volume of investigated zone.}$

The latent heat of solidification (L) is a crucial component in the determination of the true temperature field. Due to the formation of nuclei at the onset of the liquidus temperature the fraction solid (V_s) changes as the temperature drops. This increase in nuclei formation increase the heat generated due to formation of nuclei which briefly increases the temperature.

Without taking the second boundary condition, also known as the Neumann condition or heat flux, into account the cooling curve will be represented in Figure 2.1(I). The true solidification curve is represented in Figure 2.1(II). The phenomenon that occurs from B to D is particularly important for micro modelling. However, only the macro model will be considered for this investigation.

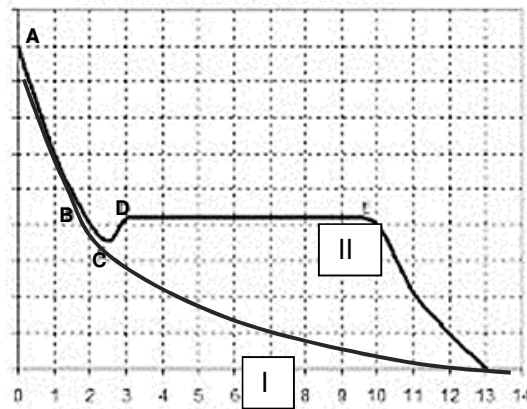


Figure 2.1 - Graph illustrating the effect of latent heat of solidification on the final temperature of the casting.

Consequently the energy equation for the mould can also be considered

$$C_m(T) \frac{\partial T_m}{\partial \tau} = \nabla [\lambda_m(T) \cdot \nabla T] \quad (2)$$

where $m = \text{mould identifier}$

The Robin boundary condition is applied to the surface of the mould. Although the surroundings to the solution space is not investigated, the surface temperature is affected by convection at the mould/air interface. For the purposes of this investigation natural convection will be considered.

The convection on the surface of the mould (in this instance) can be represented by equation 3:

$$-\lambda_m(T) \cdot \frac{\partial T}{\partial n} = \alpha(T_m - T_a) \quad (3)$$

where $\alpha = \text{convection coefficient } (W/(m^2 \cdot K))$

$T_a = \text{ambient temperature } (K)$

$T_m = \text{temperature on mold surface } (K)$

$n = \text{normal vector derivative}$

At the interfaces between mould/insulation and mould/casting the fourth boundary condition is considered as a rule with constant contact between surfaces and given by equation 4.

$$\lambda(T) \cdot \frac{\partial T}{\partial n} = -\lambda_m(T) \cdot \frac{\partial T_m}{\partial n} \quad (4)$$

Another major factor to consider for heat transfer between the component and the feeding channels in the investment casting tree is radiation. Radiation is a method of heat transfer that does not rely on the flow of material, nor does it rely on the heated surfaces being in contact such as in the case of the above mentioned convection and conduction processes.

The heat generated as a function of the cooling metal is dissipated in the form of radiation energy to the surrounding surfaces which in this case is neighbouring cast components. Consequently, in any numerical simulation of an investment mould the radiation interchange between these surfaces must be taken into account. The view factor is defined as the fraction of total radiant energy leaving one surface that arrives at another surface. The view factor is purely a function of geometry.

Heat can be transmitted through empty space by thermal radiation, also called infrared radiation or electromagnetic radiation.

The complex geometry, closely orientated components and the thin walled mould results in excessive radiation that affects the rate of heat loss.

To consider thermal radiation one must describe the solution space as a series of bodies, some radiating heat while others absorb it. In the case where all radiation is absorbed by a body

it is known as a black body or an ideal body, but this does not exist in nature. For non-ideal bodies the radiation is partly reflected absorbed or transmitted and is called irradiation.

The net radiation heat loss rate in a body when the surrounds are cooler, can be expressed with equation 5.

$$-\lambda_m(T) \cdot \frac{\partial T}{\partial n} = \varepsilon(T_m^4 - T_a^4) \quad (5)$$

where ε = emissivity of the object (one for a black body). Generally this value is between 0 and 1 depending on material and temperature of surface.

Additionally the angle at which the radiated heat leaves body one and at which it meets body two influences that accumulates heat and can be expressed by Lambert's Cosine Law illustrated in equation 6:

$$\sigma_\beta = q \cos\beta \quad (6)$$

where σ_β = *heat emission in angle β*

q = *heat emission from the surface*

β = *angle*

A cross section through the top of the investment tree is illustrated in Figure 2.2. The components with their respective inlet feeders are arranged with their centres on equilateral triangles. The radiation heat flow is relatively complicated due to complex geometry. For example, the radiation heat flow leaving the surface of one component, may or may not be intercepted by surrounding components. Also, the components are considered to be non-black or grey bodies, which means that not all radiation energy that falls on them are absorbed, but could also be reflected or transmitted. This radiation heat flow can be reflected multiple times before all energy is finally absorbed.

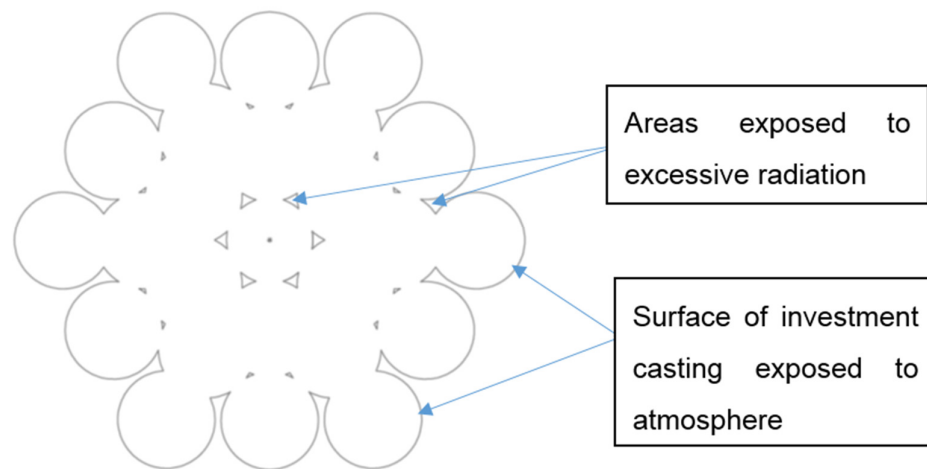


Figure 2.2 Investment casting top section through inlet feeders indicating radiation analysis.

For viewing of these complex calculations standalone software such as Facets™ are utilised. These standalone software packages allow for the optimisation of the geometry to either reduce or increase radiation effects to specific areas. Built-in modules in Magmasoft™ and Solidworks™ uses radiation calculations to determine heat flow results, but the user is unable to view such calculations for optimisation processes.

2.3 Thermo-physical parameters

The thermo-physical parameters are the characteristics of how a material behaves when it is subjected to temperature and these parameters are the density, thermal conductivity, specific heat, fraction solid and latent heat of solidification of the material. These parameters are temperature and material dependent excluding latent heat of solidification which is a given material constant.

2.4 Initial conditions

Initial conditions are the conditions at time(t) = t_0 for the set of mathematical equations. Initial conditions are required across entire solutions space. These values represent the known values of the given problem and are required to solve the mathematical model. Initial temperatures of the metal, mould and surroundings are employed at the onset of the numerical

simulation. The metal and mould are transient state condition and the surroundings are steady state and also forms the boundary of the solution space.

2.5 The Numerical Model

The goal of the numerical model is to produce an accurate representation of all the physics of the casting process and allow the user to adjust and effectively control the process parameters. By visualising the processes the user is able to see problems such as porosity, temperature gradients, metal flow, solidification fronts and distortion and make adjustments to remove these defects. Bonollo and Odorizzi [13], however, stated that the reliability of such simulations are closely linked to the initial boundary conditions and knowledge of the materials involved in the simulation, and that making poor decisions on the input data will result in misleading results.

Making use of such software and numerical simulation reduces overall manufacturing cost by reducing the trail-and-error period of design especially with expensive pattern and mould manufacturing.

To simplify discussion surrounding the methods of solution we can consider a one-dimensional solution space $T(x, t)$ with a set of points $x_i, i = 1, 2, 3 \dots N$ in the domain of $T(x)$ (refer to Figure 2.3) The numerical solution that we are looking for is represented by the function values $\{T_1, T_2, \dots, T_n\}$ at the discrete points. It will also be assumed that the space is equally discretised with constant distance between the nodes unless otherwise stated.

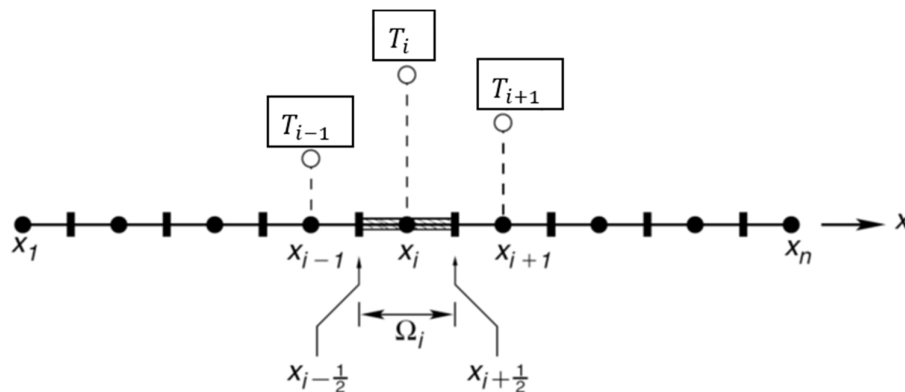


Figure 2.3 - Discretised space of the domain.

There are many situations where obtaining the exact solution is not possible and we have to make approximations. The process of obtaining a finite set of data points involve obtaining values from the continuous solution and representing these values in a finite set. This set of Partial Differential Equations (PDEs) is called a discrete system. After the set of PDEs are obtained the process of obtaining values can be completed using one of the following methods.

- Finite Difference Method
- Finite Element Method
- Control Volume Method
- Least squares Method
- Galerkin Method
- Collocation Method
- Boundary Element Method etc.

The two most common are discussed in the following sections.

2.5.1 The Finite Difference Method

The following numerical approximations will be written in differential form. It is also possible to approximate the solutions using integral form and Weighted Residual Method (WRM), but they are not discussed in this section. Please refer to further reading by Mochnacki et al. for detailed explanation of this method. The following section briefly describes this process. The first step is to approximate the derivatives into discrete functions or finite differences. Equation 7 illustrates the Taylor series that is an expansion of the Euler method.

$$T(x) = T(x_0) + T'(x_0) \frac{(x-x_0)}{1!} + T''(x_0) \frac{(x-x_0)^2}{2!} + \dots \quad (7)$$

Now donating $x_0 = x_i$ and $x = x_{i+1}$ or $x = x_{i-1}$ and considering only the first three terms we can rewrite the Taylor series as follows

$$f(x_{i+1}) = f(x_i) + f'(x_i)(x_{i+1} - x_i) + f''(x_i) \left(\frac{(x_{i+1} - x_i)^2}{2!} \right) \text{ and} \quad (8)$$

$$f(x_{i-1}) = f(x_i) - f'(x_i)(x_{i+1} - x_i) + f''(x_i) \left(\frac{(x_{i+1} - x_i)^2}{2!} \right) \quad (9)$$

where x_i = the value of x at investigated node
 x_{i+1} = the value of x at the next node adjacent to x_i

Below is an illustration of the explicit scheme utilised in finite difference method. Implicit and generalised schemes are also well used in industry, but not discussed in this section. Equation 10 illustrates the forward differential scheme that donates the temperature gradient over time.

$$\left(\frac{\partial T}{\partial t}\right) \approx \frac{T_i^{n+1} - T_i^n}{\Delta t} \quad (10)$$

Equation 11 represents the central differential scheme for the second order derivative for change of temperature over a discrete distance.

$$\left(\frac{\partial^2 T}{\partial x^2}\right) \approx \frac{T_{i+1}^t - 2T_i^t + T_{i-1}^t}{x^2}, \quad (11)$$

The algebraic procedure to derive equation 10 and 11 from equation 9 has been purposely ommited. Refer to readings of Mochnacki et al.

Equation 10 and 11 are incorporated into the mathematical model (equation 1 from previous section) and represented in equation 12 below. Here it can be noticed that the temperature at any point i in the next time step $f+1$ be easily obtained from the surrounding nodes at this time step f .

$$\frac{T_i^{n+1} - T_i^n}{\Delta t} = \alpha \left(\frac{T_{i+1}^t - 2T_i^t + T_{i-1}^t}{x^2} \right) + q_i, \quad (12)$$

where α = thermal diffusivity
 q_i = heat flux

The discrete functions can now be represented in global matrix notation through the method of lines. Equation 13 illustrates the matrix notation. And from here the temperatures can be easily found for each node.

$$\frac{d}{dt} \begin{bmatrix} T_2 \\ T_3 \\ \dots \\ T_{n-2} \\ T_{n-1} \end{bmatrix} = \frac{\alpha}{\Delta x^2} \begin{bmatrix} -2 & 1 & & & \\ 1 & -2 & 1 & & \\ & 1 & -2 & 1 & \\ & & 1 & -2 & 1 \\ & & & 1 & -2 \end{bmatrix} \begin{bmatrix} T_2 \\ T_3 \\ \dots \\ T_{n-2} \\ T_{n-1} \end{bmatrix} + \begin{bmatrix} q_2 + \frac{\alpha 1(t)}{\Delta x^2} \\ \vdots \\ \vdots \\ q_{N-1} + \frac{\alpha 2(t)}{\Delta x^2} \end{bmatrix} \quad (13)$$

Or in matrix notation

$$\frac{dT}{dt}(t) = A T(t) + q_i(t), \quad (14)$$

The main disadvantage to the FDM method is the restriction to simple geometry. Complex geometry cannot be accurately discretised into equally size elements especially in complex geometry and errors especially at the boundaries are prone to occur. The only method to improve accuracy at boundaries or at specific locations is to increase number of nodes and subsequent cells or to employ an additional method called CVM. This increase in nodal density, although it is not specific to investigated area, but will be increased along the x-, y- and z-coordinate system for the entire mesh over the investigated area. This phenomenon can be easily visualised in the casting, insulation and shell section view Figure 2.4. Mesh in rectangular marked section is refined and due to this, the cells along the x and y axis are also refined resulting in additional computing time.

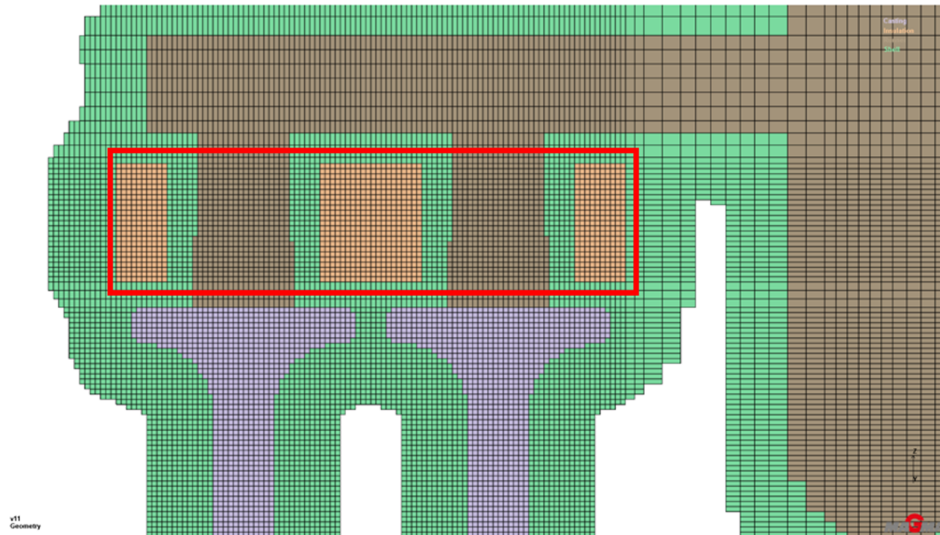


Figure 2.4 - FDM investigated space with mesh.

The numerical equations are simple and numerical processing fast to perform multiple iterations, however, the accuracy of final results is strongly depended on the mesh refinement.

2.5.2 The Finite Element Method (Galerkin)

The finite element method is based on the WRM, making use of integrals parts, as appose to the differential form of WRM for FDM. For ease of explanation equation 1 in section 2.2 will be utilised with boundary conditions $x = 0: \phi \left(T, \frac{dT}{dx} \right) = 0, x = L: \phi \left(T, \frac{dT}{dx} \right) = 0$

$$\int_0^L \left[\frac{d}{dx} \left(\lambda \frac{dT}{dx} \right) \right] + q_v w dx + \int_0^L q_v w dx = 0 \quad (15)$$

We then integrate by parts to obtain a weak formulation of the WRM illustrated in equation 16

$$q(0)w(0) - q(L)w(L) - \int_0^L \lambda \frac{dT}{dx} \frac{dw}{dx} dx + \int_0^L q_v w dx = 0 \quad (16)$$

The next step divide the solution space into finite elements that is interconnect by nodes as illustrated in Figure 2.3. Let the distance between nodes be denoted as h .

Therefore the temperature at x .

$$T(x) = \frac{1}{h}(x_i - x)T_{i-1} + \frac{1}{h}(x - x_{i-1})T_i, \quad (17)$$

where $\frac{1}{h}(x_i - x) = N_i$ and $\frac{1}{h}(x - x_{i-1}) = N_{i-1}$ which is called *shape* functions.

For Galerkin method the shape functions are equal to the weight functions as described in equation 18.

$$w(x) = N_{i-1}\beta_{i-1} + N_i\beta_i, \quad (18)$$

where β_i and β_{i-1} are coefficients of the base functions

Once the derivatives for all the shape functions calculated over each element as been determined (illustrated in equation 19 and 20) the matrices can be combined into a global stiffness matrix from where the temperature values can be calculated. The mathematical process to find equations 19 and 20 has been purposefully omitted.

$$\int \lambda \frac{dT}{dx} \frac{dw}{dx} dx = \frac{\lambda}{h} [\beta_i, \beta_{i-1}] \begin{bmatrix} 1 & -1 \\ -1 & 1 \end{bmatrix} \begin{Bmatrix} T_i \\ T_{i-1} \end{Bmatrix} \quad (19)$$

and

$$\int q_v w dx = \frac{q_v h}{2} [\beta_i, \beta_{i-1}] \begin{Bmatrix} 1 \\ 1 \end{Bmatrix} \quad (20)$$

FEM unlike FDM is numerically stable which means that any errors obtained in the input and calculations do not accumulate with the subsequent iterations.

Additionally with FEM complex geometry can be easily meshed by accurately interpreting the boundary with finite elements. In FEM the solution space is discretised into elements that accurately depict the solution space and the discretisation error is less. The use of triangular or tetrahedral elements are most common in FEM space.

Where FDM makes use of the strong differential form of governing equations, FEM makes use of the integral or WRM method mentioned earlier. The use of integral method is more advantages as it is a more natural approach to Neumann boundary conditions. FEM is therefore also more suited to deal with complex geometries and multi-dimensional problems as the shape of the mesh is not important.

Figure 2.5 illustrates the difference between meshing in FDM and FEM respectively.

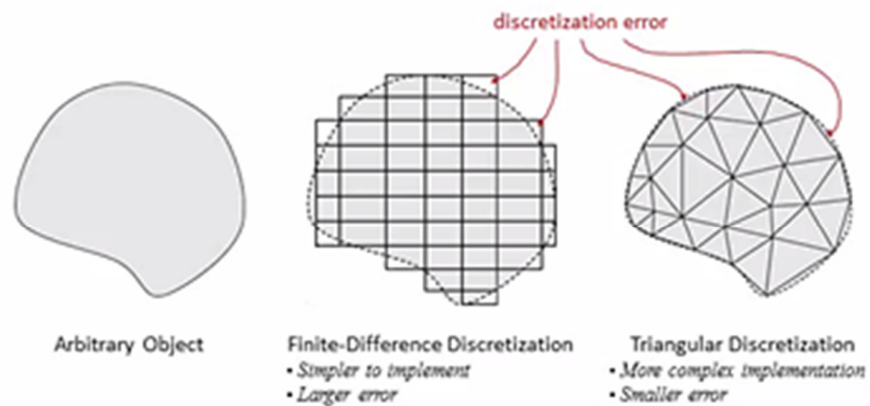


Figure 2.5 - Illustrating the difference in meshing in the FEM and FDM space.

3. Numerical Investigation of the investment casting process

3.1 The Geometric Model

The model was generated using DSS Solidworks™ software. The single valve was defined as the final model for use in all subsequent cases. The valve component is illustrated in Figure 3.1 with the following overall dimensions.

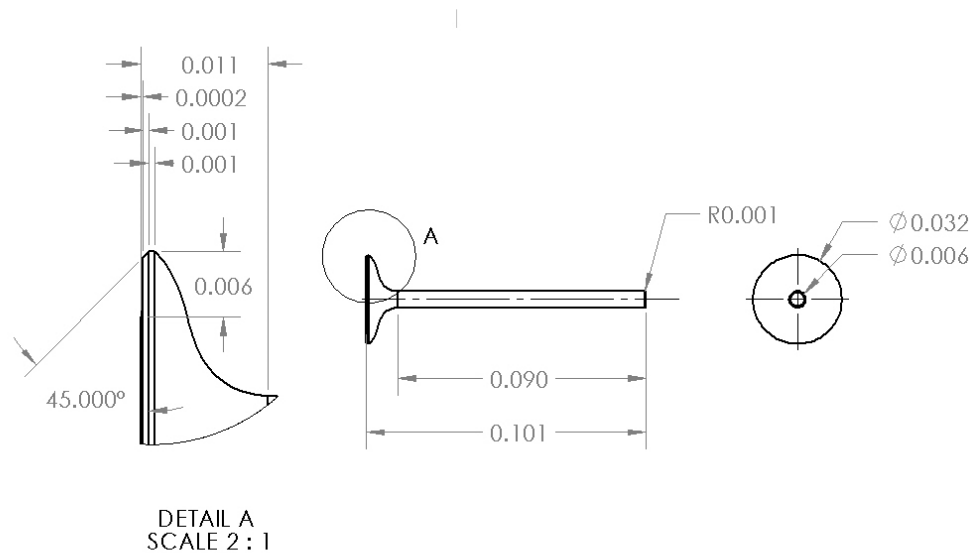


Figure 3.1 Manufacturing drawing of investigated inlet valve

3.2 Investment casting gating system design calculations

To design the investment casting tree the following calculations must be followed. The values obtained, however, are only a guideline along which the geometry must be designed. Due to external factors such as geometric complexity that influences factors such as cooling rates, small geometric and parameters changes should be made to improve flow and solidification conditions.

3.2.1 Volume of the casting

$$V = \pi r^2 * l \quad (21)$$

where $V = \text{volume of casting}$
 $r = \text{radius of casting}$
 $l = \text{length of casting}$

therefore $V = \pi * [(2.7^2) * 0.45] * 10^{-6} + \pi[(0.35^2) * 9.6] * 10^{-6}$
 $V = (3.694 + 2.770) * 10^{-6}$
 $V = 6.464 * 10^{-6} m^3$

3.2.2 Mass of component

$$m = V * \rho \quad (22)$$

where $m = \text{mass of casting}$
 $\rho = \text{density}$

therefore $m = (3.694 + 2.770) * 10^{-6} * 4430$
 $m = 0.029 kg$

3.2.3 Modulus of the component

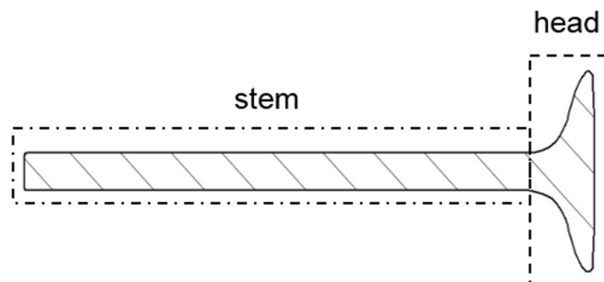


Figure 3.2 - Sectioned valve.

$$M = \frac{V}{CS} \tag{23}$$

where $M = \text{modulus}$
 $CS = \text{casting surface (m}^2\text{)}$

therefore
$$M_{stem} = \frac{\pi r^2 * l}{(2\pi r * l) + 2\pi r^2}$$

$$M_{stem} = \frac{3.695 * 10^{-6}}{(0.211 + 0.077) * 10^{-6}}$$

$$M_{stem} = 1.689$$

$$M_{head} = \frac{\pi r^2 * l}{(2\pi r * l) + 2\pi r^2}$$

$$M_{head} = \frac{2.771 * 10^{-6}}{(1.232 + 0.396) * 10^{-6}}$$

$$M_{head} = 1.703$$

3.2.4 Feeder and downsprue modulus

The values for the feeder modulus is obtained from Table 3.1 and used in equation 24 to determine the downsprue modulus.

Table 3.1 - Table used to determine modules of feeder [77].

Component weight in grams	Type of Parameter	Parameter value for “m”				
		1.1	1.8	2.5	3	3.5
50	D _{wg} mm	20	20	25	25	30
	M _{ZS} for l _{ZS} of 4mm	1.75	2.5	2.7	3.3	3.5
	M _{ZS} for l _{ZS} of 8mm	2	<u>3</u>	3.2	3.5	3.75
51-100	D _{wg} mm	20	20	25	30	30
	M _{ZS} for l _{ZS} of 4mm	2	2.75	3	3	3.5
	M _{ZS} for l _{ZS} of 8mm	2.5	3.25	3.5	3.75	4.3
101-200	D _{wg} mm	20	25	30	30	35
	M _{ZS} for l _{ZS} of 4mm	2.5	2.5	3	3.25	3.75
	M _{ZS} for l _{ZS} of 8mm	3	3.5	3.75	4.25	4.5

Values obtained from Table 3.1

$$l_{zs} = 8mm$$

$$m = 1.8mm$$

$$D_{wg} = 20mm$$

$$m_{zs} = 3 \text{ (From table above)}$$

$$m_{wg} = \frac{2^4 \sqrt{m^3 G} \sqrt[3]{l_{zs}}}{m_{zs}} \quad (24)$$

where m_{zs} – module of feeder
 m_{wg} – module of downsprue
 m – module of casting
 G – weight of casting
 l_{zs} – length of feeder

therefore
$$m_{wg} = \frac{2^4 \sqrt{1.695^3 * 29} \sqrt[3]{8}}{3}$$

$$m_{wg} = 4.59$$

3.2.5 Nominal downsprue diameter

$$m_{zs} = \frac{v}{CS} \quad (25)$$

therefore
$$m_{zs} = \frac{\frac{\pi * D_z^2}{4} * l_{zs}}{\pi * D_z * l_{zs}} = \frac{D_z^2}{4D_z} = \frac{D_z}{4}$$

$$D_z = 4 * m_{zs} = 3 * 4$$

$$D_z = 12mm$$

Table 3.2 - Data used to determine diameter and length of downsprue [77].

Type of sprue	Diameter of sprue (mm)	Length of sprue (mm)				
		250	280	320	360	400
Cross-section (D)	20	+		+		
	25		+	+		
	32		+	+	+	

From Table 3.2 the nominal diameter and length for the downsprue for successful pour is 20mm and 320mm respectively.

To predict a successful pour the following conditions must be satisfied:

$$m_{wg} > m_{zs} > m$$

Using above calculated modulus from equation 19 and 20 it can be seen that the conditions are met.

$$4.6 > 3 > 1.65$$

3.2.6 Optimal flow velocity

$$v_p = k_4 \frac{l_{max}}{g_0} \quad (26)$$

where k – 0.05 if flooding from above, 0.06 from side, and 0.08 from bottom.
 l_{max} – the maximum length of the thinnest wall in mm,
 g – the thickness of the most thinnest wall in mm.

therefore
$$v_p = k_4 \frac{l_{max}}{g_0} = 0.05 * \frac{96}{7} = 0.685 \text{ kg/s}$$

3.2.7 Minimum safe diameter through which the material can flow

$$f_{min} = \frac{23 * v_p}{\mu * \gamma * \sqrt{H_m}} \quad (27)$$

and

$$H_m = \rho gh, \quad (28)$$

where H_m – pressure of the metal in the thinnest wall
 μ – flow coefficient (for a laminar flow of 0.8 – 0.9, the dynamic flow 1.4 – 1.5)

γ – density of the metal in g/cm³.

therefore $H_m = 4.43 * 9.81 * 0.35 = 15.21$

and

$$f_{min} = \frac{23 * 0.685}{1.5 * 4.5 * \sqrt{15.21}}$$

$$f_{min} = 0.598 * 10^{-4} m^2$$

From the values obtained from equation 29 the minimum diameter through which the metal can flow is determined

$$D_{zmin} = \sqrt{\frac{4 * f_{min}}{\pi}} \quad (29)$$

where $D_{zmin} = \text{minimum diameter (m}^2\text{)}$

$$\text{therefore } D_{zmin} = \sqrt{\frac{4 * f_{min}}{\pi}} = 0.873 * 10^{-4} m^2$$

3.3 Numerical Analysis:

According to literature, porosity is the main defect observed in castings and for this reason it was decided to investigate amendments to the geometry, and initial and boundary conditions. Amendments made to these points previously mentioned and the effect to the properties of the component would be analysed. The localised investigations were performed on a single inlet feeder and component. This process took into consideration the pouring and solidification process where factors such as shrinkage porosity and temperature gradients are analysed. This investigation was subdivided into nine distinct sub-categories as illustrated in Table 3.3.

Table 3.3 - Illustration of localised investigations on the inlet feeder and component.

Case nr.	Alterations performed to geometry and parameters	Constraints
1	Component orientation from 0 to 90° in increments of 10°.	Diameter and length of inlet feeder remains constant
2	Length of inlet feeder from 5 to 23mm in increments of 2mm.	Diameter and modulus remains constant
3	Change of diameter from 6 to 24mm in increments of 2mm.	Length remains constant
4	Inlet feeder angle from 0 to 45° in increments of 5°.	Inlet diameter remains constant
5	Five shapes of inlet feeder	Modulus remains constant
6	Diameter of the insulation around the feeder from 24 to 36mm in increments of 2mm.	Inlet feeder remains constant
7	Initial inlet temperature from 1690 to 1740°C in increments of 5°C.	All geometrical parameters remains constant
8	Feeding time from 1 to 4s in increments of 0.25s.	All geometrical parameters remains constant
9	Mould temperature from 300 to 1000°C in increments of 50°C.	All geometrical parameters remained constant

3.3.1 Analysis for individual inlet geometry

The following cases investigate individual pouring and solidification parameters. In all cases only a single parameter was altered to establish its relationship to numerical results. By adjusting only a single parameter the student could understand the relationship of the alteration to the occurring defects. All boundary conditions are constant and applicable as discussed in chapter two across the entire investigation.

Ambient temperature changes were not investigated and was assumed constant at 20°C across all investigations.

3.3.1.1 Change of component orientation

For case 1 the component geometrical orientation was altered to determine its relationship with numerical results specifically component soundness, porosity and hot spot location. Numerical simulation initial conditions and geometry are illustrated in Table 3.4.

Table 3.4 - Initial and boundary conditions for change of component orientation.

Description	Value
Pouring temperature	1740°C
Mould temperature	600°C
Pouring time	2s
Component orientation	Altered
Inlet feeder shape	Cylindrical
Inlet feeder diameter	12mm
Inlet feeder length	24mm
Inlet feeder orientation	Altered as a result of component orientation
Inlet feeder modulus	3mm

3.3.1.1.1 Geometrical set-up

For case 1 the angle of the component geometry was altered from 0° to 90° in 10° increments. 0° represents vertically orientated component.

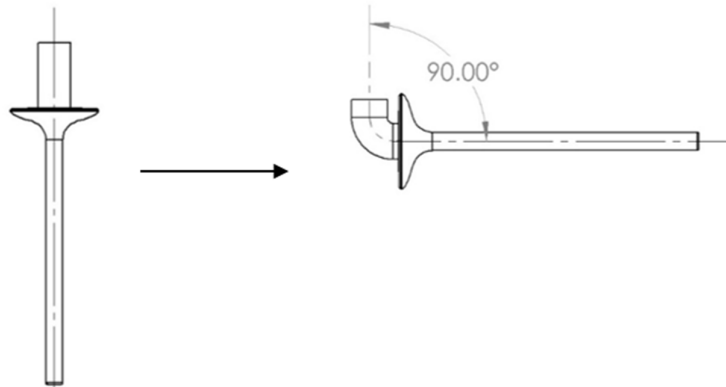


Figure 3.3 - Geometrical set-up and illustration of alteration to component angle from 0 to 90°.

3.3.1.1.2 Results

Hotspot formation at the surface of the component is observed in numerical results from simulation software. Alteration to component angle altered porosity probability and position as illustrated in Figure 3.4 and Figure 3.5.

For case 1 it was observed that at 0° and 90° less than 5% porosity in the stem of the component is observed. At any angle between 0° and 90° the probably of porosity is observed with a maximum at 45° showing exponential proportionality as illustrated in Figure 3.4. Also it

is shown in Figure 3.5 that the position of the porosity observed in the inlet feeder moves along the length of the inlet feeder proportional to the probability found in Figure 3.4. Best results are obtained at 0° and 90° intervals.

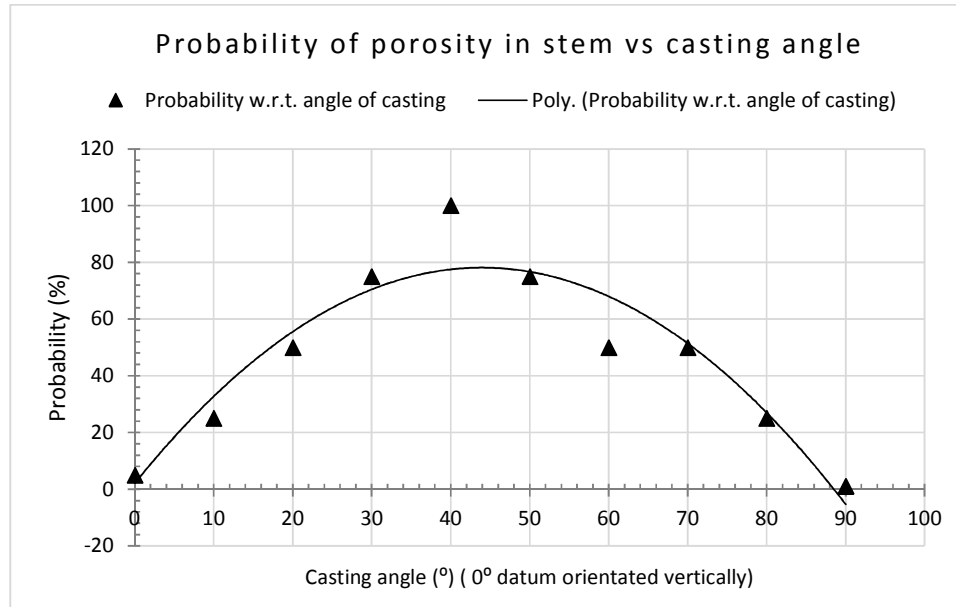


Figure 3.4 - Probability of occurrence of porosity with respect to change of component geometrical orientation from 0 to 90°.

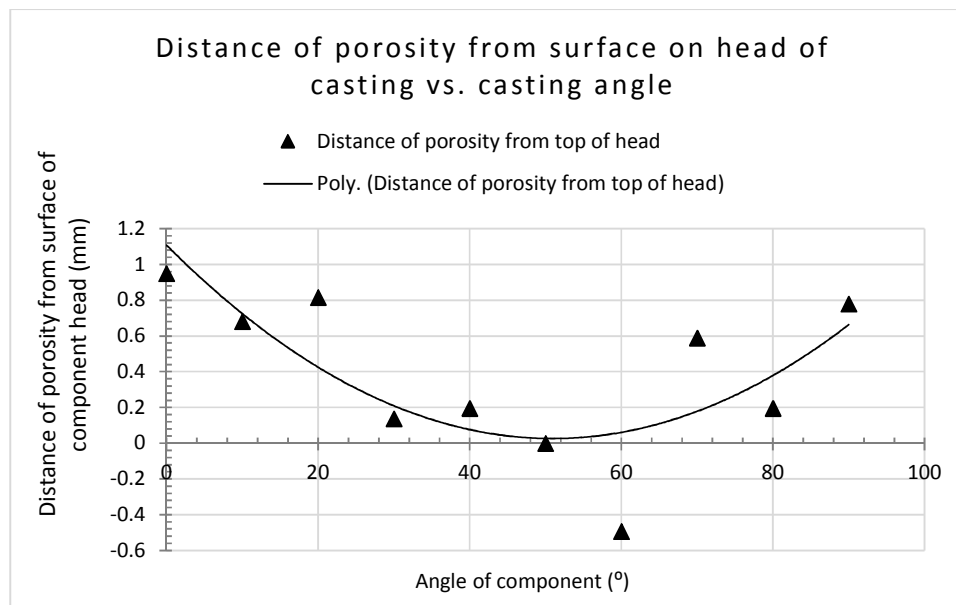


Figure 3.5 - Change of porosity with respect to change of component geometrical orientation from 0 to 90°.

Five thermocouples was placed along the centreline from the surface of the component head in 3mm increments. This thermocouple set-up is used across all investigated cases.

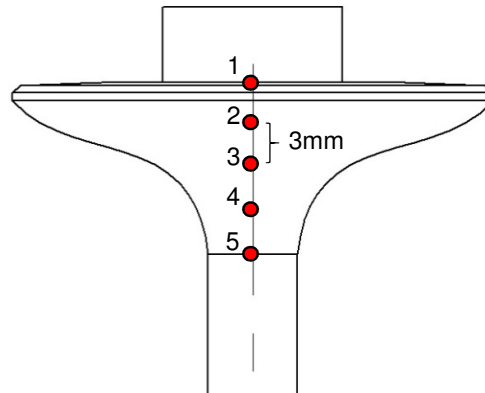


Figure 3.6 - Thermocouple positions located along the centreline of the component.

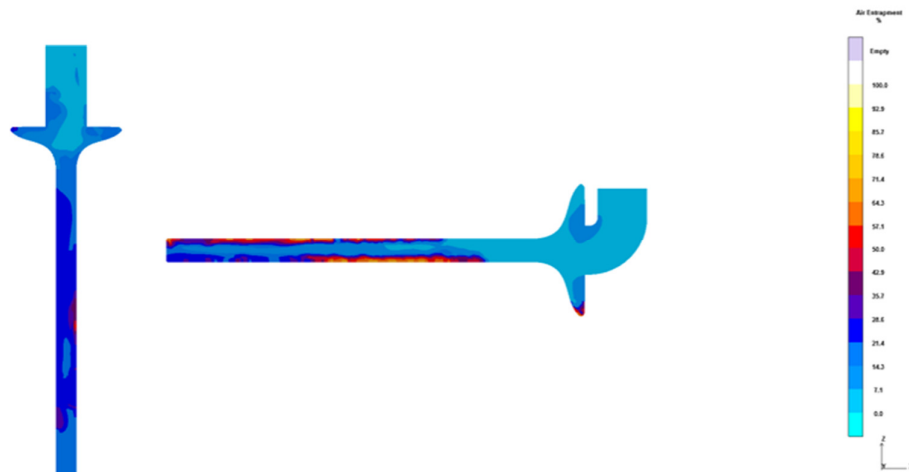


Figure 3.7 - Air Entrapment in the component at 0 and 90° respectively.

3.3.1.1.3 Conclusion

Alteration to the component geometry angle as significant effects to the probability to formation of porosity in the stem of the component. At 0° and 90° orientation the best results was obtained. At interstitial increments, between 0° and 90°, the effect of porosity could lead to

microstructural changes that has not been investigated. Future work should employ investigations into the microstructural changes.

The position and occurrence of porosity affected the temperature gradient and cooling rate inside the head of the component at the onset of solidification at all increments.

It was found that severe air entrapment was observed for the component orientated at 90° as illustrated in Figure 3.7. This entrapment will cause surface porosity, undesirable dimensional changes and rough surface quality. The component orientated at 0° indicates up to 50% probability of air entrapment, however, 70% of component indicated probability below 25%. The best orientation was decided to be vertically orientated under current component conditions. Subsequent investigations will therefore be performed with the component vertically orientated.

3.3.1.2 Change of inlet length

For case 2 the inlet geometry length was altered to determine its relationship with numerical results specifically component soundness, porosity and hot spot location. Numerical simulation initial and geometric conditions are illustrated in Table 3.5.

Table 3.5 - Initial and geometric conditions for change of inlet length.

Description	Value
Pouring temperature	1740°C
Mould temperature	600°C
Pouring time	2s
Component orientation	Vertical
Inlet feeder shape	Cylindrical
Inlet feeder diameter	12mm
Inlet feeder length	Altered
Inlet feeder orientation	Vertical
Inlet feeder modulus	3mm

3.3.1.2.1 Geometrical set-up

For case 2 the length of the inlet feeder was altered in increments of 2mm from 5 to 23mm as illustrated in Figure 3.4.

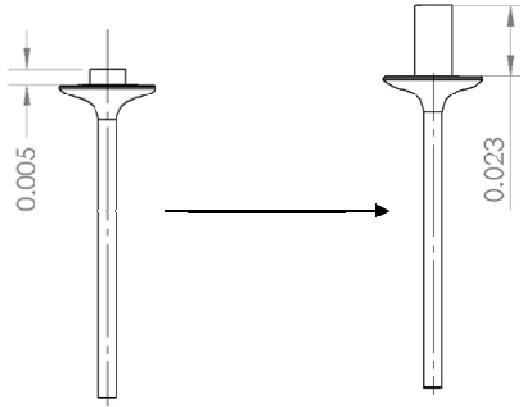


Figure 3.4 - Alteration of inlet length from 5mm to 23mm.

3.3.1.2.2 Results

For case 2 excessive porosity occurred in the inlet feeder close to the surface of the casting head. Alteration to the inlet length only accounted for slight changes in porosity severity and position.

Porosity occurrence in the stem of the casting remained constant and was observed along the centreline of the casting.

Porosity distance from the surface of head of casting was measured for all 10 instances of case 2. The results was collated and represented in Figure 3.5.

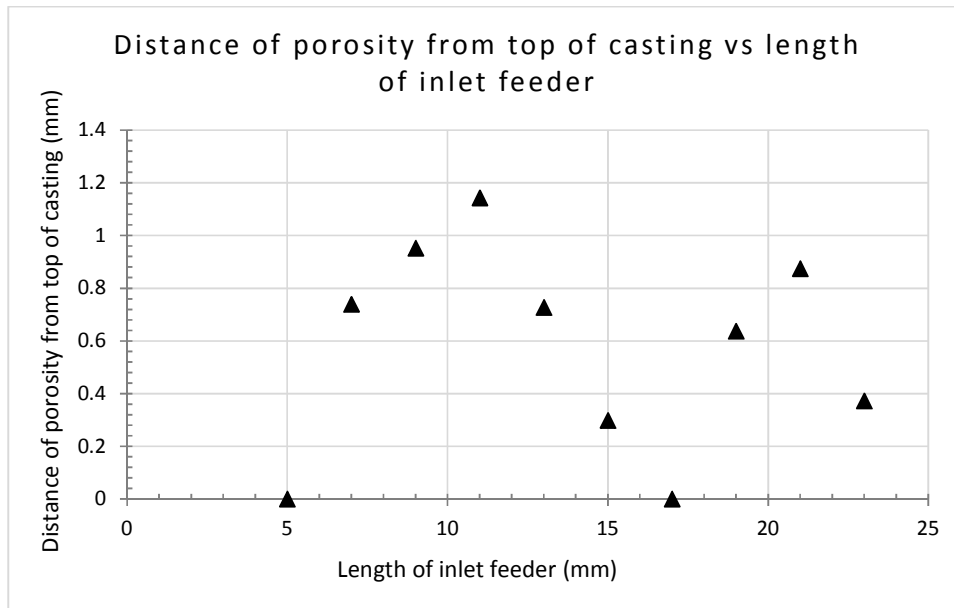


Figure 3.5 - Graph representing distance of porosity from surface of casting head.

3.3.1.2.3 Conclusion

Porosity was observed at the surface of the casting and the porosity did not protrude into the casting. Alteration to the inlet length changed the position of the porosity, but not to any beneficial extent. No relationship between the data points were observed. The inlet length had no observable effects on the temperature gradient and subsequent cooling rates at the surface and inside the head of the casting. Solidification will proceed unaffected. Amount of simulations must be increased to determine validity of results and to find relationship.

3.3.1.3 Change of inlet diameter

For case 3 the inlet geometry diameter was altered to determine its relationship with numerical results specifically component soundness, porosity and hot spot location. Numerical simulation initial and geometric conditions are illustrated in Table 3.6.

Table 3.6 - Initial and geometric conditions for change of inlet diameter.

Description	Value
Pouring temperature	1740°C
Mould temperature	600°C
Pouring time	2s
Component orientation	Vertical
Inlet feeder shape	Cylindrical
Inlet feeder diameter	Altered
Inlet feeder orientation	Vertical
Inlet feeder length	20mm
Inlet feeder modulus	3mm

3.3.1.3.1 Geometric set-up

For case 3 the diameter of the inlet feeder was altered in increments of 2mm from 6 to 24mm as illustrated in Figure 3.6.

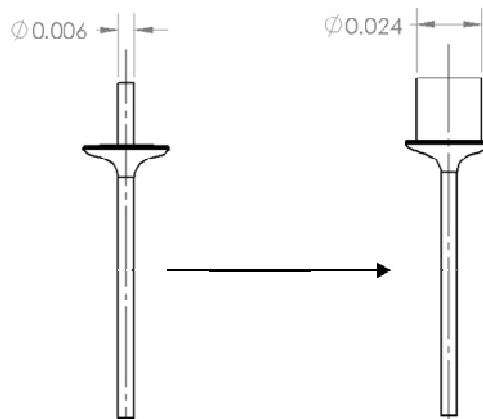


Figure 3.6 - Geometrical set-up and alteration of inlet geometry diameter for Case 3.

3.3.1.3.2 Results

For case 3 porosity occurred in the inlet feeder and inside the head of the component. Alteration to the inlet feeder diameter and consequent modulus showed beneficial improvements to the location of the porosity (refer to Figure 3.7). Overall soundness and hotspot location, which is directly related to occurrence of porosity, also showed improvement. Minor porosity occurrence in the stem of the component remained constant and was observed along the centreline of the component.

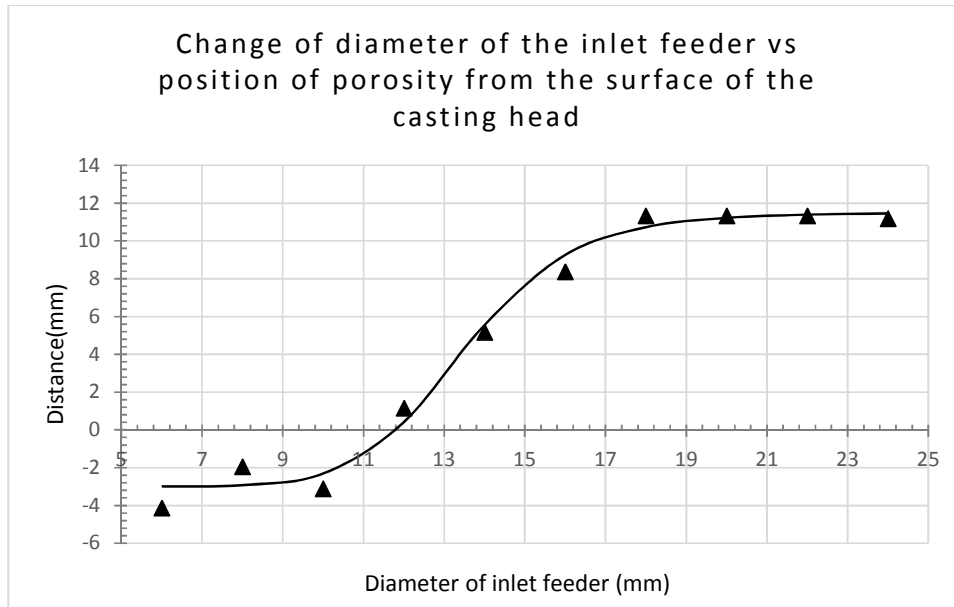


Figure 3.7 - Change of porosity with respect to change of diameter of inlet feeder.

The distribution in Figure 3.7 is best represented by a generalisation of the sigmoid function. This function is effective for coordinates that do not cross the X-axis at the origin, but are offset. Equation 30 represents the fitted generalised sigmoidal curve.

$$y = D + \frac{(A-D)}{1 + \left(\frac{x}{C}\right)^B}, \quad (30)$$

where A is minimum value of the function
 B is the maximum slope of the function
 C is the point of inflection
 D is the maximum value of the function

therefore
$$y = 11.5 + \frac{-(4+11.5)}{1 + \left(\frac{x}{13.5}\right)^{10}}$$

Above values were obtained through the use of an optimisation algorithm in Microsoft Excel for a best fit curve. Values were rounded for simplicity.

Temperature gradient curves for both thermocouple 1 and 2 illustrates the effect with the change of diameter. The occurrence of porosity on or around the thermocouples acts as an energy reservoir which adversely affects the cooling curve readings.

The phenomenon can be illustrated in Figure 3.8 and Figure 3.9.

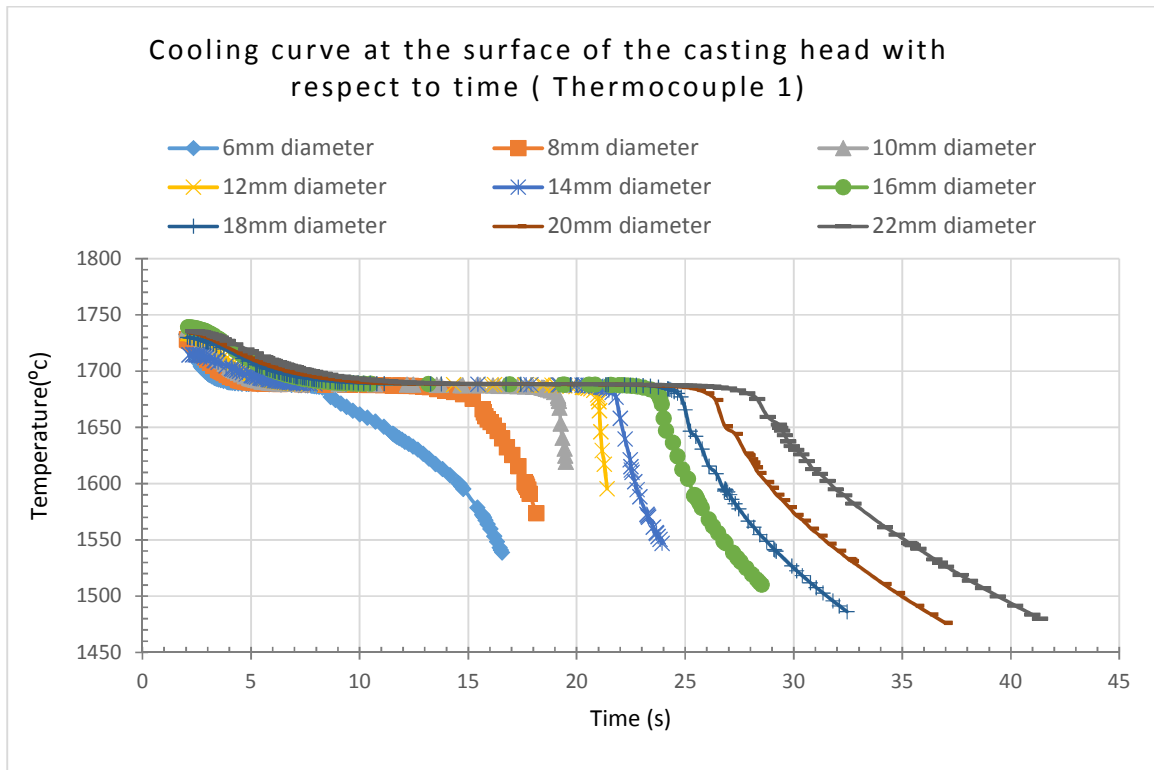


Figure 3.8 - Temperature distribution at thermocouple (1) for Case 3 from 6mm to 22mm inlet feeder diameter.

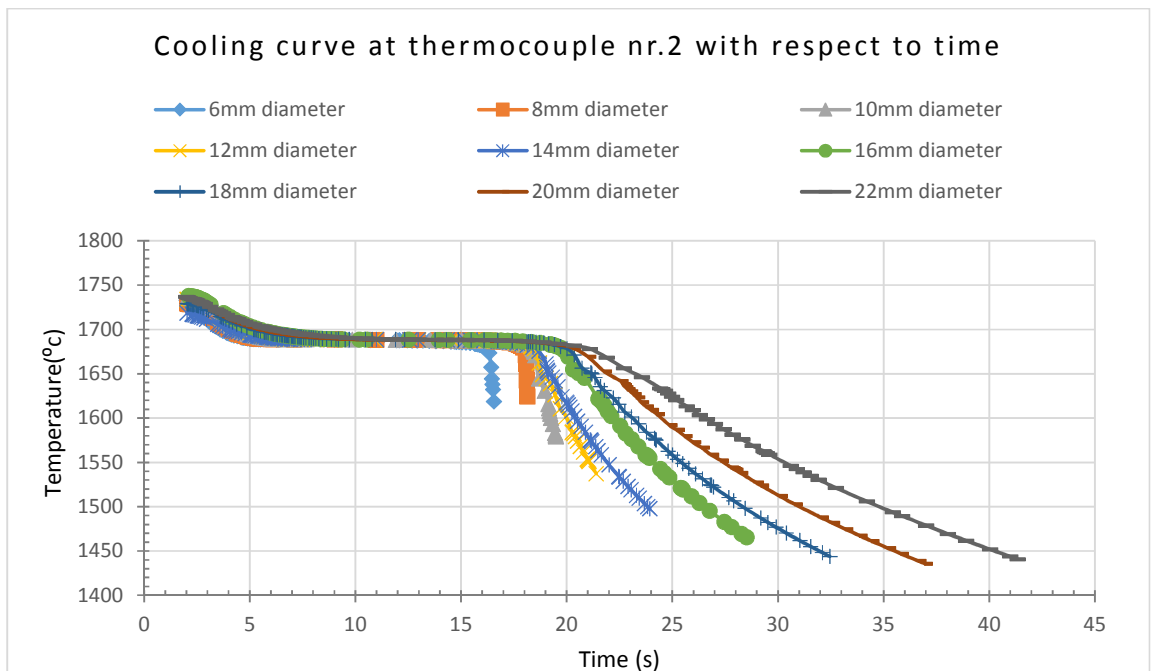


Figure 3.9 – Cooling curves at thermocouple (2) for Case 3 for 6mm to 22mm inlet feeder diameter.

Cooling rates observed in the $\phi 14\text{mm}$ inlet feeder is in the order of 95°K/s compared to cooling rates observed in the 22mm inlet feeder that reaches a maximum of 37°K/s .

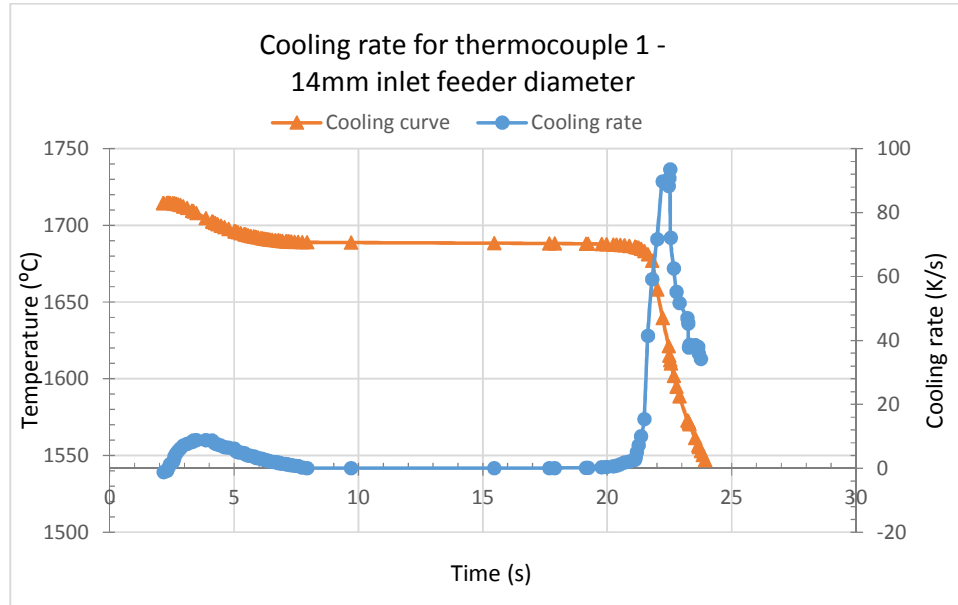


Figure 3.10 – Cooling curve and cooling rates for thermocouple 1 - 14mm inlet feeder diameter.

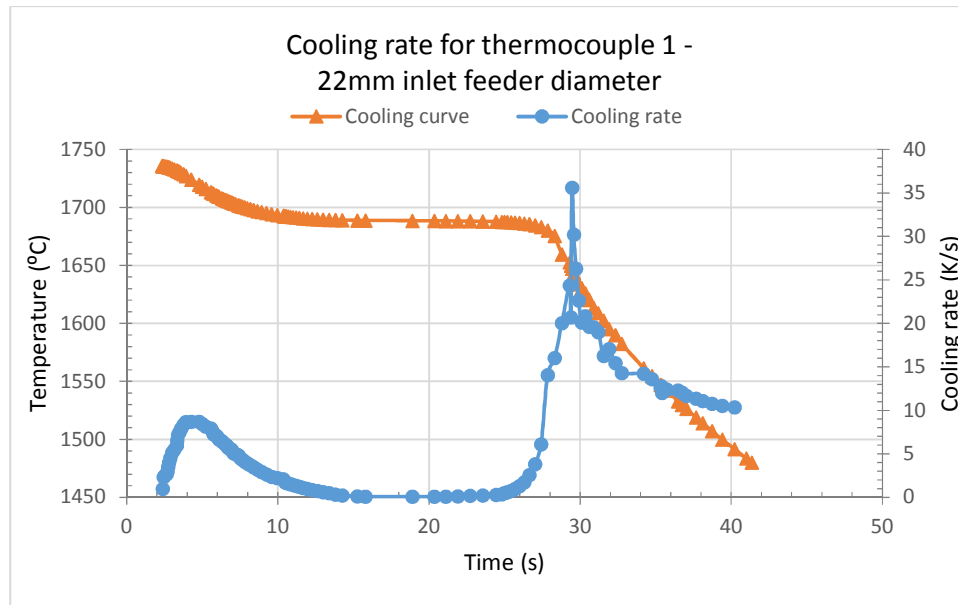


Figure 3.11 - Cooling curve and cooling rates for thermocouple 1 - 22mm inlet feeder diameter.

3.3.1.3.3 Conclusion

Porosity was observed in the inlet feeder, on the surface and inside the head of the component for $\phi 6\text{mm}$ inlet feeder. As the diameter was increased the position of the porosity was altered and showed beneficial results. The relationship between the diameter and the position of porosity followed a generalised sigmoid function.

This slower cooling rate observed in Figure 3.11 leads to longer cooling times at the surface of the component head. This effect could lead to microstructural changes that must be further investigated to determine the effect on mechanical properties.

3.3.1.4 Change of inlet feeder shape

For case 4 the inlet geometry shape was altered to determine its relationship with numerical results specifically component soundness, porosity and hot spot location. Numerical simulation initial and geometrical conditions are illustrated in Table 3.7.

Table 3.7 - Initial and geometric conditions for change of inlet feeder shape.

Description	Value
Pouring temperature	1740°C
Mould temperature	600°C
Pouring time	2s
Component orientation	Vertical
Inlet feeder shape	Altered
Inlet feeder diameter	12mm
Inlet feeder length	23mm
Inlet feeder orientation	Vertical
Inlet feeder modulus	3mm

3.3.1.4.1 Geometrical set-up

For this geometrical set-up five main geometrical shapes was investigated. For the conical inlet a modulus of 3mm was unable to be attained and by constraining the overall height dimension to that of the cylinder the modulus was 5mm.

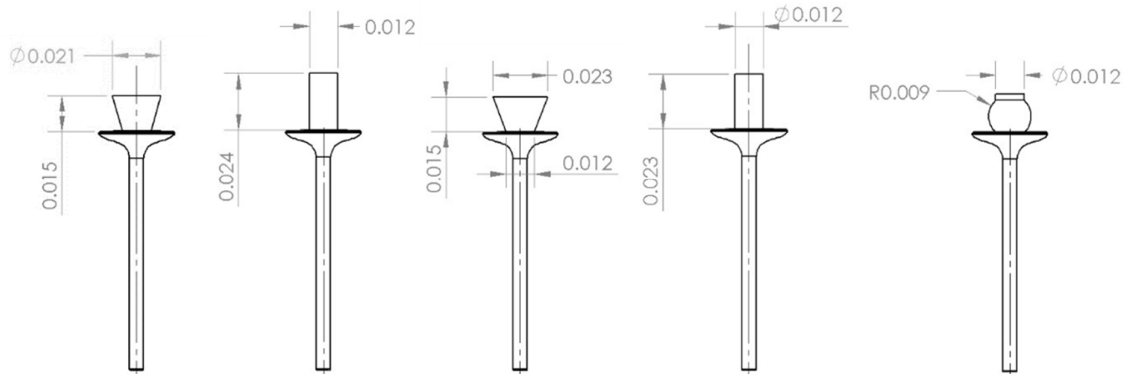


Figure 3.12 - Illustration of the shapes of inlet feeder under investigation.

3.3.1.4.2 Results

Figure 3.13 is a representation of the position of porosity with respect to the shape of the inlet geometry. For each instance the occurrence of porosity closest to the surface of the head of component was logged and illustrated.

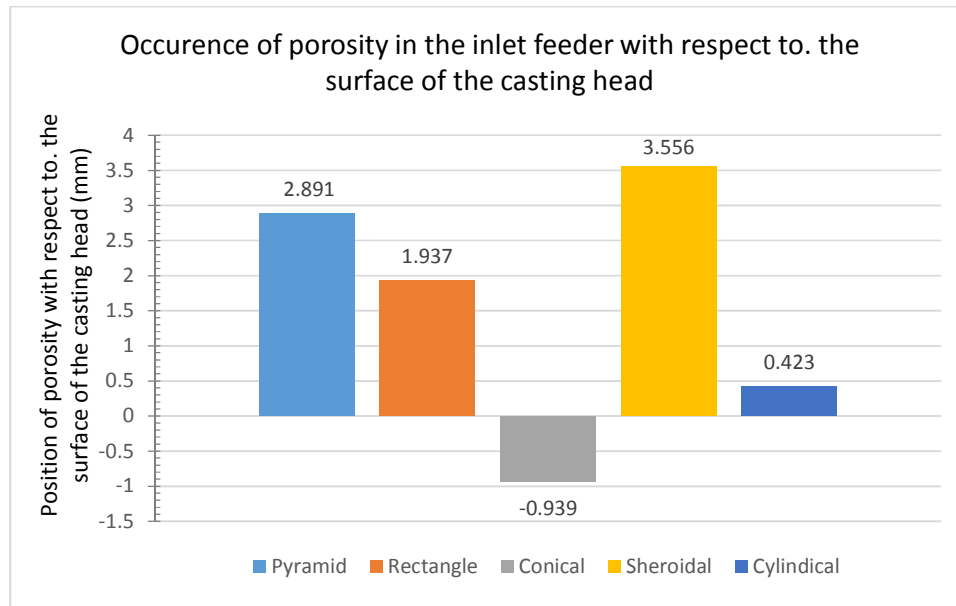


Figure 3.13 – Position of porosity on the surface of the head of the component with respect to inlet feeder shape.

3.3.1.4.3 Conclusion

It was observed that the pyramid and spheroidal inlet feeder produced soundest components without porosity in the head or on the surface of the components. Also spheroidal and pyramid inlet geometries yielded unaffected temperature gradients on the surface of the component. However, due to change in modulus of the conical shape these results cannot be compared accurately.

Due to difficulty of producing inlet feeder geometries of unique shapes it is unlikely that such shapes will be used in industry. The results do indicate that different shapes of same modulus yields significantly different results.

3.3.1.5 Change of inlet angle

For case 5 the inlet feeder angle was altered to determine its relationship with numerical results specifically component soundness, porosity and hot spot location. Numerical simulation initial and geometric conditions are illustrated in Table 3.8.

Table 3.8 - Initial and geometric conditions for change of inlet angle.

Description	Value
Pouring temperature	1740°C
Mould temperature	600°C
Pouring time	2s
Component orientation	Vertical
Inlet feeder shape	Cylindrical
Inlet feeder diameter	12mm
Inlet feeder length	23mm
Inlet feeder orientation	Altered
Inlet feeder modulus	3mm

3.3.1.5.1 Geometrical set-up

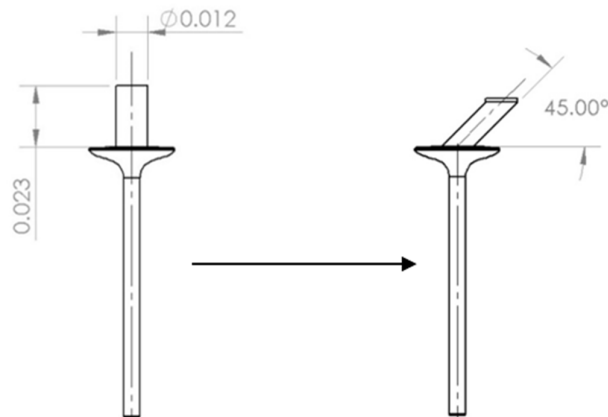


Figure 3.14 - Geometrical set-up and alteration of inlet angle for case 5.

3.3.1.5.2 Results

Figure 3.15 is a representation of the position of porosity with respect to the change of the inlet angle. For each instance the occurrence of porosity closest to the surface of the head of component was logged and illustrated.

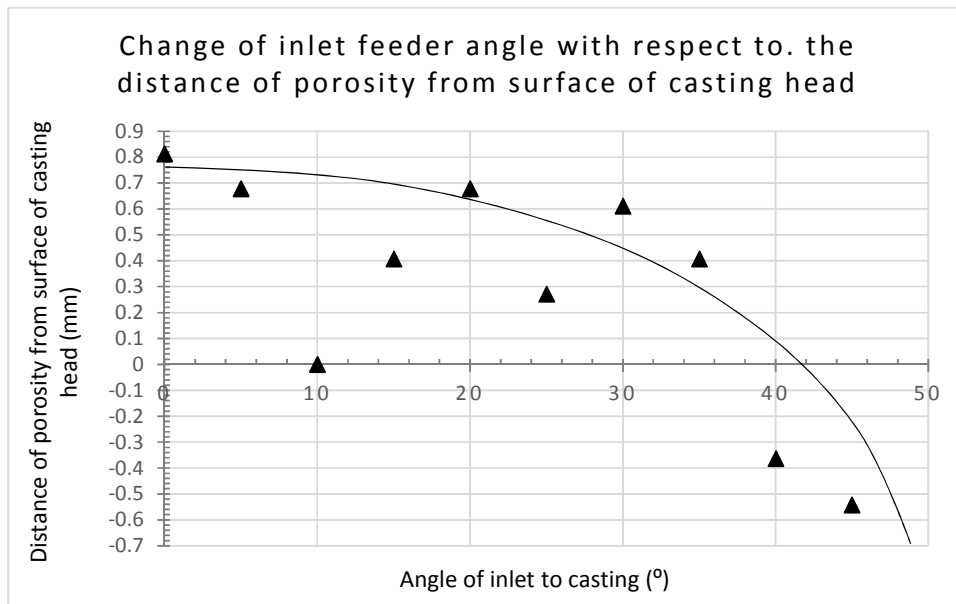


Figure 3.15 - Effect of change of inlet angle to position of porosity.

3.3.1.5.3 Conclusions

It can be observed that at 0°, a vertically orientated inlet feeder, the porosity in the feeder is furthest away from the component head.

As the angle is increased the tendency is for the porosity to 'move' towards the component surface head (negative gradient) as observed in proposed relationship in Figure 3.15. The investigated range is less than 2mm, and the results could therefore be a result of noise. The true relationship, if any, is not fully understood, but a tendency for porosity to move from the inlet feeder to the head of component is observed.

3.3.1.6 Addition of insulation and change of insulation diameter

For case 6 the component geometrical was orientated in a vertical position and was unaltered. Insulation was added to the inlet feeder and the outer diameter was incrementally increased to see the effect on the start of solidification, and to determine its relationship with numerical results specifically component soundness, porosity and hot spot location. Numerical simulation initial and geometrical conditions are illustrated in Table 3.9.

Table 3.9 - Initial and geometric conditions for addition and alteration to insulation diameter.

Description	Value
Pouring temperature	1740°C
Mould temperature	600°C
Pouring time	2s
Component orientation	Vertical
Inlet feeder shape	Cylindrical
Inlet feeder diameter	12mm
Inlet feeder length	23mm
Inlet feeder orientation	Vertical
Inlet feeder modulus	3mm
Insulation length	16mm
Insulation inside diameter	20mm
Insulation outer diameter	Altered

3.3.1.6.1 Geometrical set-up

For case 6 insulation was taken into account for the inlet feeder. The insulation outer diameter was incrementally increased by 2mm from 24mm to 36mm.

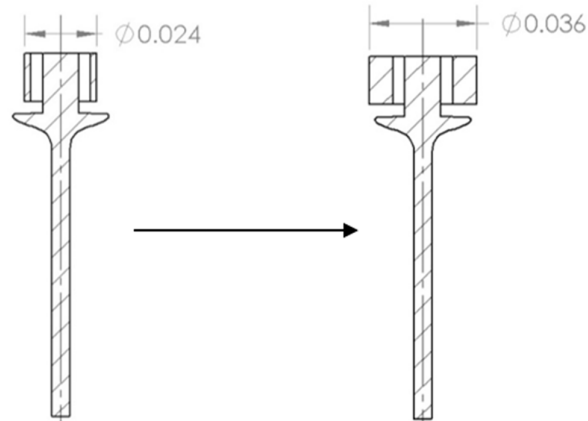


Figure 3.16 - Geometrical set-up and alteration of inlet angle diameter for case 6.

3.3.1.6.2 Results

Hotspot formation at the surface of the component and in the inlet feeder is observed in numerical results.

Minor porosity occurrence in the stem of the component remained constant and was observed along the centreline of the component.

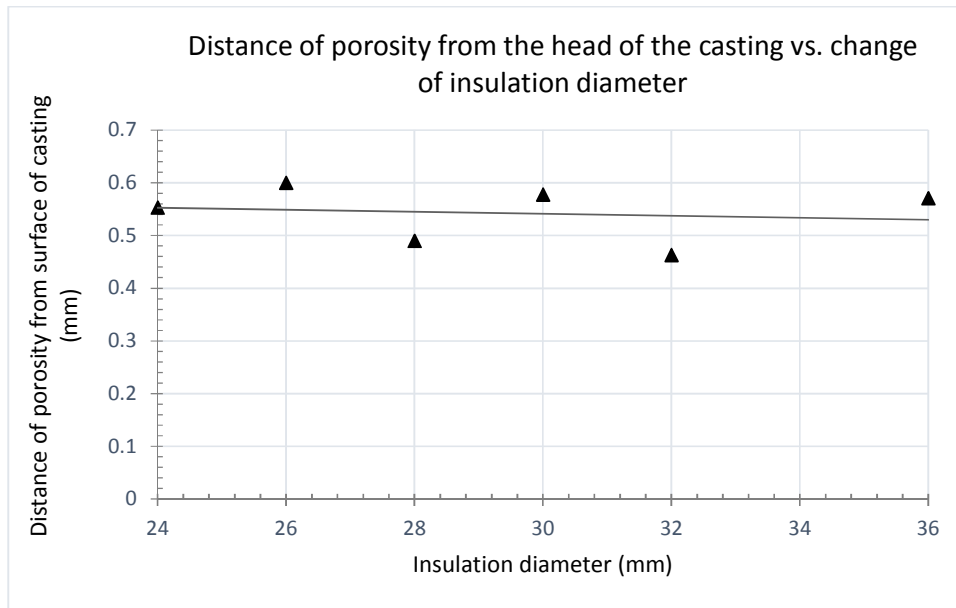


Figure 3.17 - Effect of changing insulation diameter to the position of porosity.

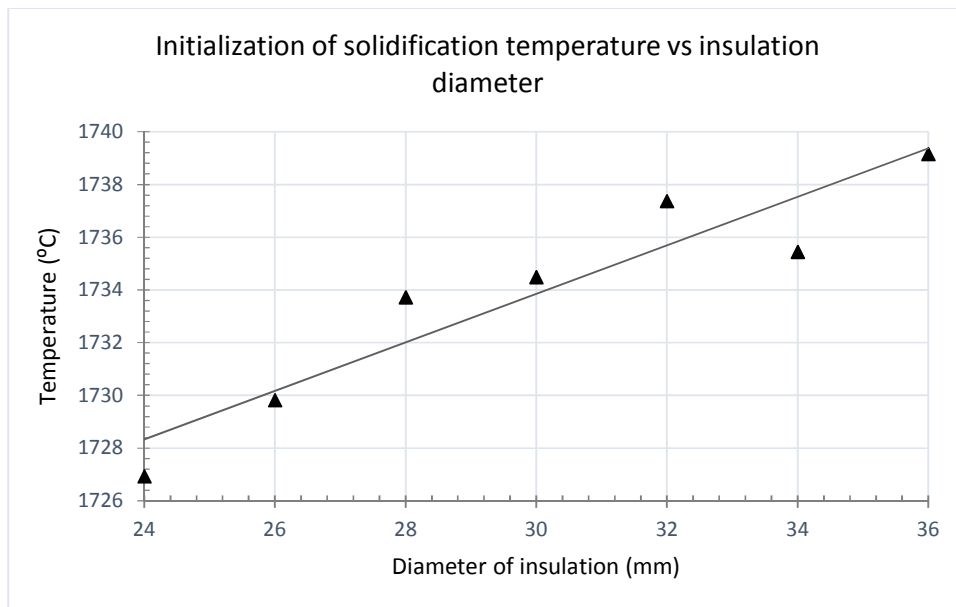


Figure 3.18 - Effect of changing insulation diameter to the solidification initiation temperature.

3.3.1.6.3 Conclusion

The alteration to the insulation diameter appeared to have little effect on the position of the hotspot as illustrated in Figure 3.17. This phenomenon is observed in similar heat flow

problems in industry. The increase in insulation diameter yields only benefit up to some point (not observed in the student's investigation) after which the increase of diameter has no effect other than additional cost to the user. This is due to the outside surface area of the insulation from which heat can radiate increases with increased diameter. Convection heat loss is a function of surface area and thus the larger the surface the more rapid the heat loss.

The change to insulation diameter has a linear tendency to increase start of solidification temperature with increased diameter. The effect on microstructure and mechanical properties is not investigated.

3.3.1.7 Change of initial temperature

For case 7 the component geometrical was orientated in a vertical position and was unaltered. The pouring temperature was incrementally increased to see the effect on the start of solidification, and to determine its relationship with numerical results specifically component soundness, porosity and hot spot location. Numerical simulation initial and geometrical conditions are illustrated in Table 3.10.

Table 3.10 - Initial and geometric conditions for change of initial pouring temperature.

Description	Value
Pouring temperature	Altered
Mould temperature	600°C
Pouring time	2s
Component orientation	Vertical
Inlet feeder shape	Cylindrical
Inlet feeder diameter	12mm
Inlet feeder length	23mm
Inlet feeder orientation	Vertical
Inlet feeder modulus	3mm

3.3.1.7.1 Geometrical set-up

For case 7 a vertical orientated component set-up was chosen. Inlet feeder was also chosen to be constant across investigation as per data in Table 3.11.

3.3.1.7.2 Results

It was observed that the position of the porosity was altered due to change to initial temperature. The overall change to porosity position was observed to be 1mm as illustrated in Figure 3.19.

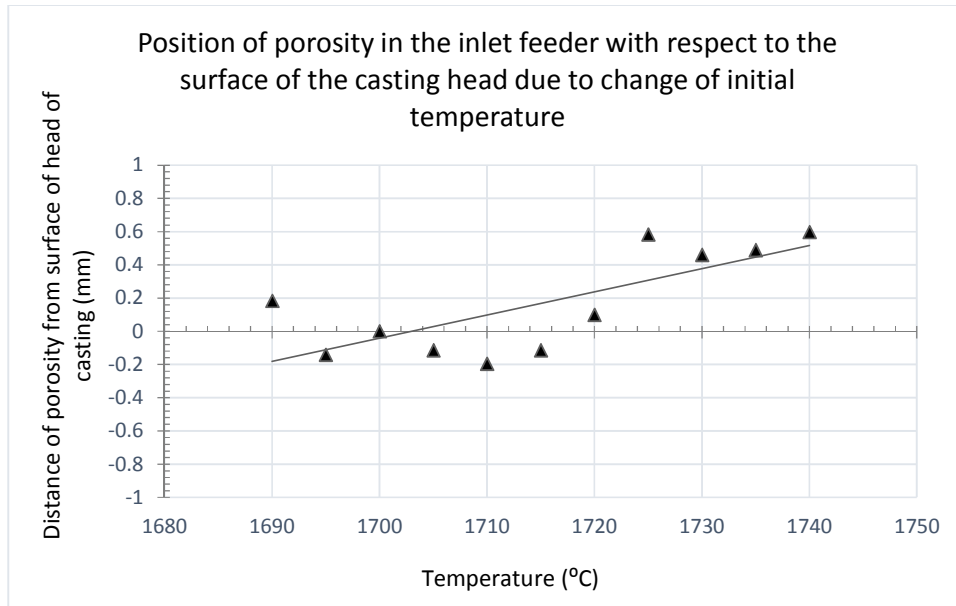


Figure 3.19 – Effect of change to initial temperature.

3.3.1.7.3 Conclusion

Alteration to the initial temperature has some effect on the position of the porosity with respect to the head of the component. Further increase of the initial temperature could yield further improvement, but according to literature, superheating titanium has no beneficial results. Titanium's low thermal diffusivity, which is a function of density, specific heat and thermal conductivity, causes titanium to solidify rapidly.

3.3.1.8 Change of pouring time

For case 8 the component geometrical was orientated in a vertical position and was unaltered. The pouring time was incrementally increased to see the effect on the start of solidification,

and to determine its relationship with numerical results specifically component soundness, porosity and hot spot location. Numerical simulation initial and geometrical conditions are illustrated in Table 3.11.

Table 3.11 - Initial and geometric conditions for change of pouring time.

Description	Value
Pouring temperature	1740°C
Mould temperature	600°C
Pouring time	Altered
Component orientation	Vertical
Inlet feeder shape	Cylindrical
Inlet feeder diameter	12mm
Inlet feeder length	23mm
Inlet feeder orientation	Vertical
Inlet feeder modulus	3mm

3.3.1.8.1 Geometrical set-up

For case 8 a vertical orientated component set-up was chosen. Inlet feeder was also chosen to be constant across investigation as per data in Table 3.11.

3.3.1.8.2 Results

Hotspot formation at the surface of the component and in the inlet feeder is observed in numerical results. The alteration to the insulation diameter appeared to have little effect on the position of the hotspot as illustrated in Figure 3.20.

Minor porosity occurrence in the stem of the component remained constant and was observed along the centreline of the component. These defects can be removed by additional post – processing techniques such as HIP.

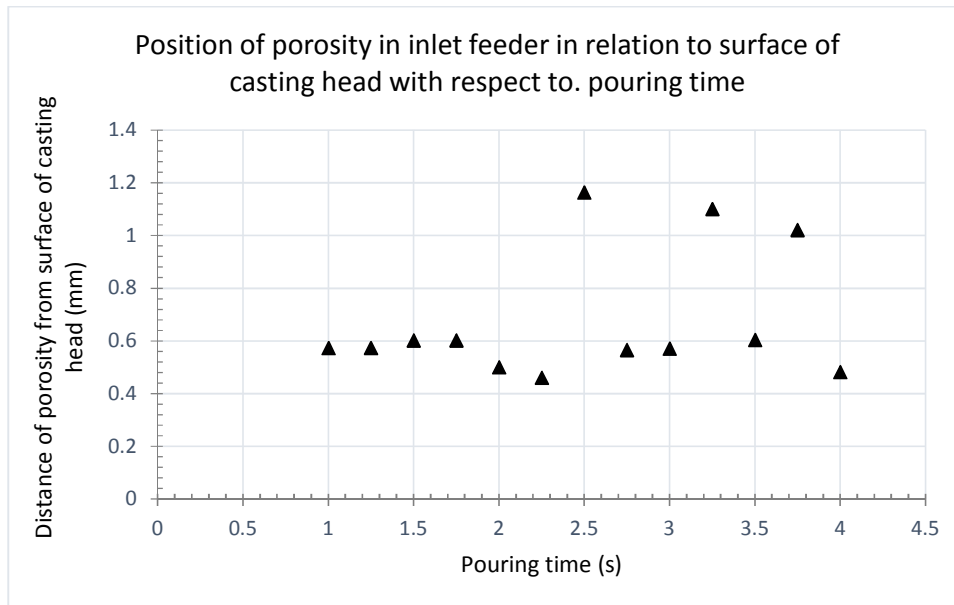


Figure 3.20 - Illustration indicating the effect of changing pouring time to the position of porosity with respect to the surface of the component head.

3.3.1.8.3 Conclusion

No relationship was found, for the range investigated, between the change of inlet temperature and the position of porosity with respect to the surface of the component head.

3.3.1.9 Change of mould temperature

For case 9 the component geometrical was orientated in a vertical position and was unaltered. The mould temperature was increased from 300 to 1000°C in 50°C increments to see the effect on the start of solidification, and to determine its relationship with numerical results specifically component soundness, porosity and hot spot location. Numerical simulation initial and geometrical conditions are illustrated in Table 3.12.

Table 3.12 - Initial and geometric conditions for change of mould temperature.

Description	Value
Pouring temperature	1740°C
Mould temperature	Altered
Pouring time	2s
Component orientation	Vertical
Inlet feeder shape	Cylindrical
Inlet feeder diameter	12mm
Inlet feeder length	20mm
Inlet feeder orientation	Vertical
Inlet feeder modulus	3mm

3.3.1.9.1 Geometrical set-up

For case 9 a vertical orientated component set-up was chosen. Inlet feeder was also chosen to be constant across investigation as per data in Table 3.12.

3.3.1.9.2 Results

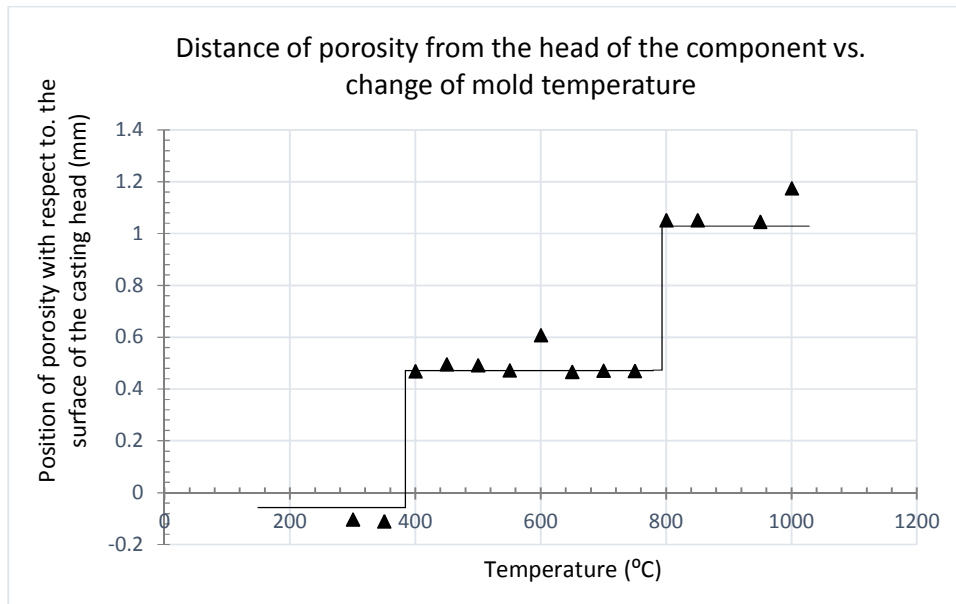


Figure 3.21 - Position of porosity with respect to the surface of the component head as mould temperature is increased.

Data points were taken across the temperature range from 300 to 1000°C and the change of porosity was observed in Figure 3.21. A distinct relationship was observed in Figure 3.22 where solidification time increased parabolically across temperature range.

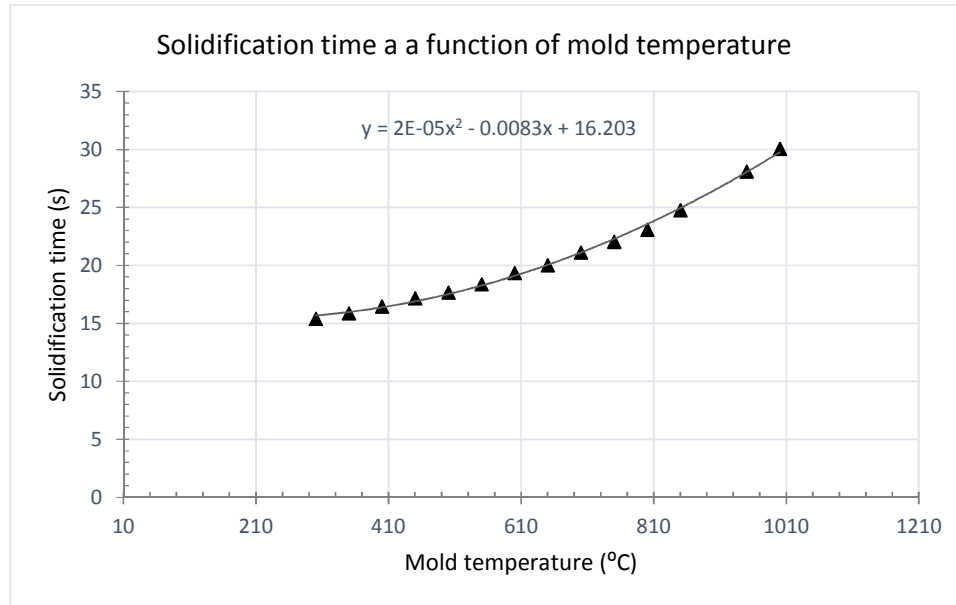


Figure 3.22 - Solidification time as a function of mould temperature.

3.3.1.9.3 Conclusion

Alteration to the mould temperature shows a step function relationship across the range of 300 to 1000°C. The movement of porosity relative to the surface of the component head is rather insignificant with only a movement of 1.4mm across a span of 700°C. Further increase of the mould temperature could yield further improvement, but according to literature and current study, a temperature of 600°C yields satisfactory results. Also the increase of mould temperature above an acceptable level becomes uneconomical.

A 2-order polynomial relationship is observed for the solidification time of the component with respect to the change of mould temperature. It can be seen that with further increase of the temperature above 1000°C less effect to change of solidification time will be observed. It then becomes uneconomical to investigate above this temperature.

4. Numerical Simulation of Casting Design

4.1 Introduction

The final gating system was designed making use of numerical results obtained from Chapter 3 for individually investigated component set-ups. The student chose the best results from each investigation and used the initial and geometrical conditions for the entire gating system. The relationships found in previous investigations completed in Chapter 3 could be used to optimise the final design in future investigations.

It is important for the student to determine the validity of combining best-fit individual results found and use this data in complex geometry. Also, the effect of complex geometry with complex flow channels and radiation plays a large role in the final microstructure and mechanical properties.

4.2 Design of casting tree

An investment casting gating system for 48 components were designed making use of results obtained in previous investigations.

The use of a cylindrical downsprue with traps distributed around the perimeter of the downsprue provides a symmetrically distributed melt. This would produce a uniform and consist solidification front in all components. The traps are rectangular to allow for ease of manufacture and assembled at a 10° angle with respect to the horizontal axis. This angle prohibits the metal melt from entering the inlet feeders prematurely as illustrated in Figure 4.1. A vertically orientated component was chosen throughout as this has beneficial properties to the removal of air, increase in metallostatic pressure in the valve stem and uniform and directional solidification.

A simple inlet feeder geometry was chosen due to ease of manufacture and assembly. The results obtained from the cylindrical inlet feeder yielded acceptable results compare to other investigated shapes. It was therefore also decided that the inlet angle should be vertical for ease of assembly. Overall dimensions of 12mm x 20mm was chosen as this yielded the best results for the smallest volume. It must be remembered that the overall volume of casting tree that does not form part of the final component reduces yield. Reduction in yield could prove that this process is uneconomical.

The alteration to pouring time yield no relationship with the position of defects and occurrence of porosity and therefore the overall pouring time will be re-calculated taking the maximum flow

rate in the thinnest section of the valve and overall volume of the casting tree into consideration.

The use of insulation has been omitted due to the fact that it has only a small effect on temperature gradient at the surface of the component head.

The mould temperature of 600°C was chosen as this temperature provided favourable results without unnecessarily overheating the mould.

The following parameters have been set out in Table 4.1 - Data obtained from individual investigation and used for final design for use in complete gating system design.

Table 4.1 - Data obtained from individual investigation and used for final design.

Description	Value
Pouring temperature	1740°C
Mould temperature	600°C
Inlet feeder shape	Cylindrical
Inlet feeder diameter	12mm
Inlet feeder length	20mm
Inlet feeder orientation	Vertical
Inlet feeder modulus	3mm
Pouring time (s)	12 seconds
Maximum yield (%)	30.8%
Valves cast (number)	48

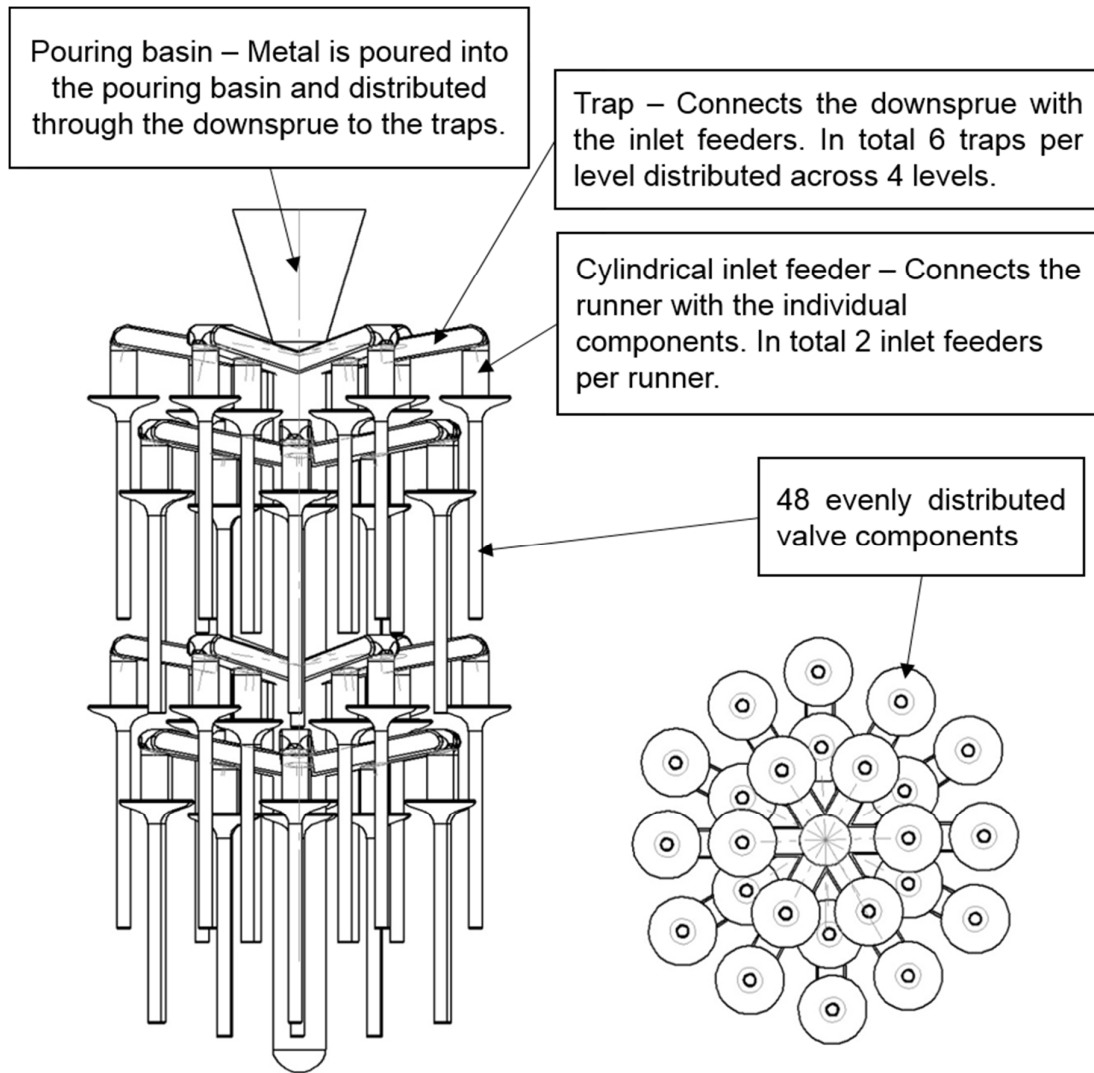


Figure 4.1 - Final design casting tree. Side and top view respectively.

4.3 Results

After final casting tree was designed numerical simulations was performed. The option to investigate simulating the pouring and solidification process for the entire casting, as appose to making use of axis of symmetry, yielded pouring properties that would otherwise not have been observed.

Overall soundness of the lower half of the casting tree can be observed in Figure 4.2. No porosity or air inclusions are observed producing maximum yield, however, the upper half of the casting tree (refer to Figure 4.3) showed signs of internal porosity in the stem that could be

removed with HIP process if not severe. Signs of porosity at the surface and in the valve component head is not observed.

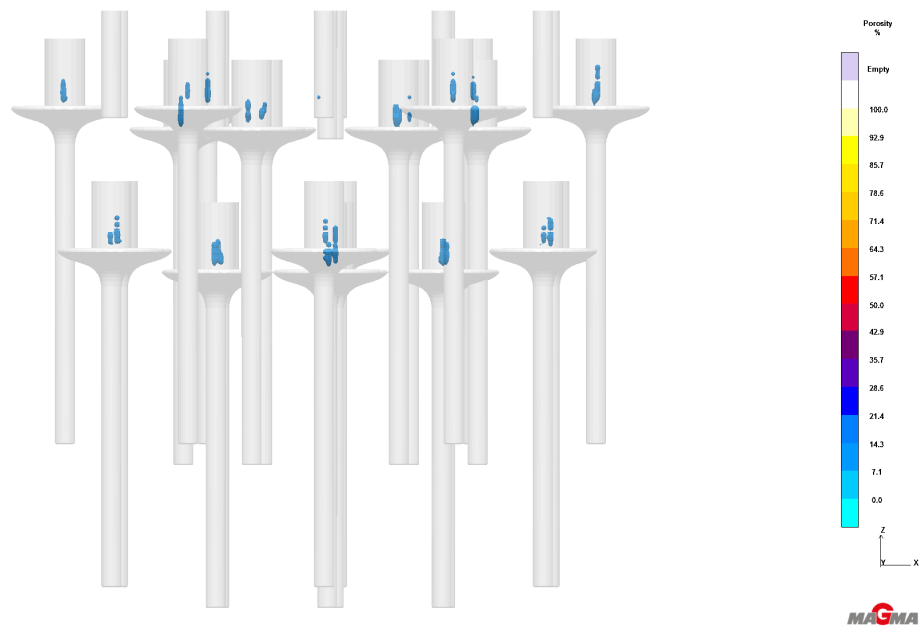


Figure 4.2 - Illustration of porosity observed in the lower half of the casting tree.

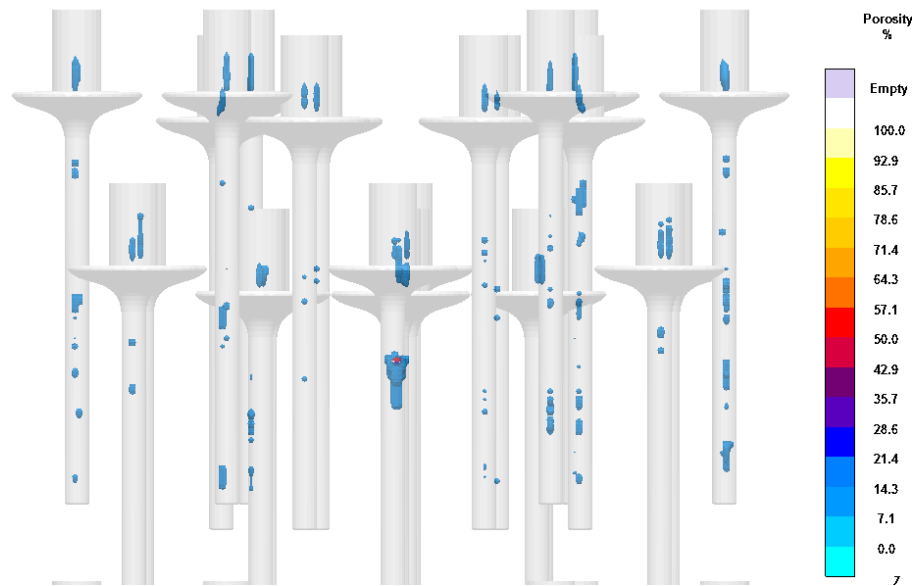


Figure 4.3 - Illustration of porosity observed in the upper half of the casting tree.

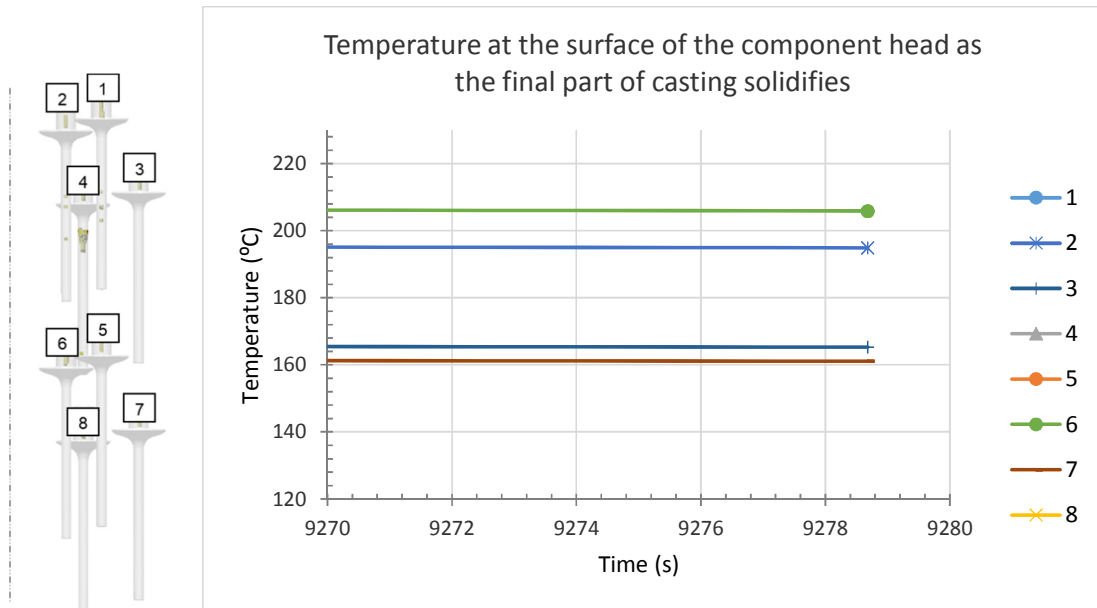


Figure 4.4 - Temperature at the surface of the valve component at the time final part of casting solidifies.

Figure 4.4 represents two distinct temperature groups are observed at the end of solidification. Casting numbers one, three, five and seven, orientated furthest away from the centreline and exposed to comparatively more ambient air, results in a final temperature of 160°C. Castings orientated closer to the centreline and exposed to radiation from surrounding valves showed an average temperature increase of 40°C. This phenomenon is further described in Figure 4.5 illustrating the cooling curves for each of these representative components of the casting tree. The components located furthest away from the centreline yielded the highest cooling rates in the order of 100°K/s indicating the effect of ambient conditions on the surface. The components located on the closest to the centreline yield cooling rates in the order of 60°K/s.

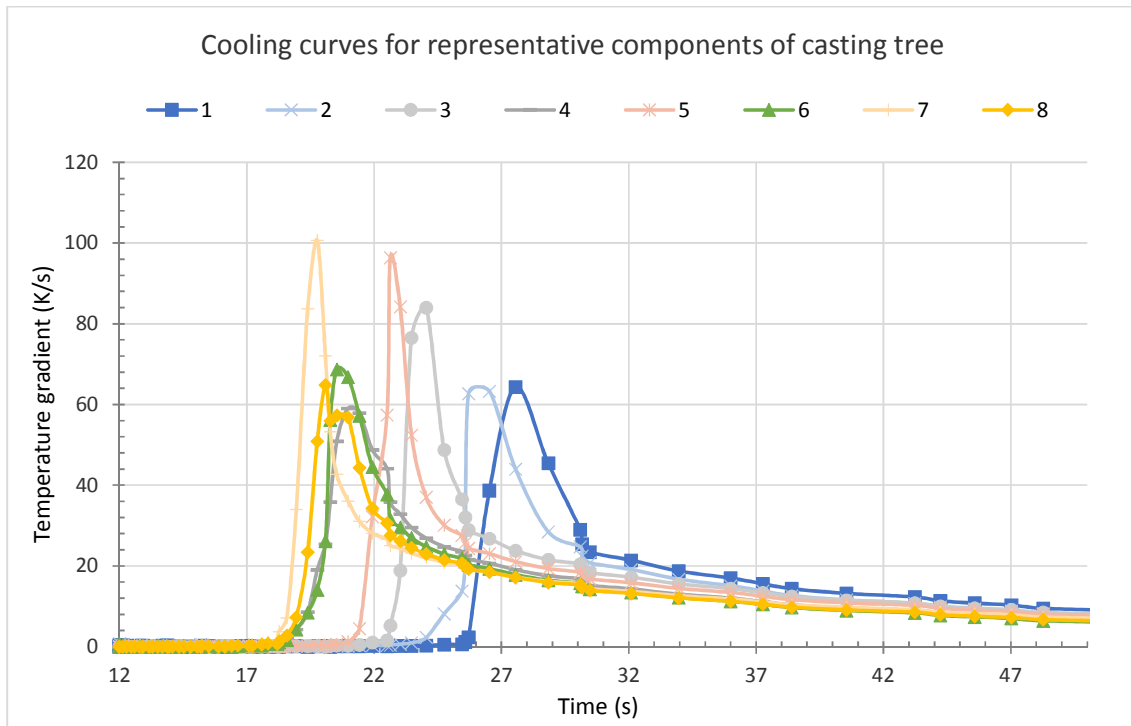


Figure 4.5 - Cooling curves for representative components for the casting tree.

4.4 Conclusions

The complexity of the final casting tree yielded results not observed in the individually assessed components. The lack of metallostatic pressure in the upper half of the casting tree reduces pressure required to remove porosity and porosity is therefore observed in all the stems in the upper half. To improve the quality of the casting the casting must be performed under centrifugal force.

The parameters in the individually investigated single casting set-up could successfully be employed in the more complex design.

Radiation plays a large role in the solidification of castings and must be investigated in future work to determine the extent of the effects.

5. Conclusions and Future Work

5.1 Conclusions

From an experimental point of view, this investigation showed that Ti6Al4V alloy, to an extent, can be successfully cast and optimised to produce a sound casting. It was observed that due to metallostatic pressure head, the casting orientated in the top half of the casting tree yielded unfavourable results. This shows that casting under gravity alone is not desired and the use of centrifugal casting for example would yield improved results. The individual parameters such as casting orientation, inlet diameter and angle, and mould temperature was altered and distinct relationships were observed. These relationships can be used for further optimisation procedures, and to investigate this, the numerical simulation must be experimentally reproduced. Final mechanical and microstructural properties must be found through mechanical tests and optical microscopy after which numerical optimisation can be performed.

The study showed that the individual parameters that influence the soundness of the casting can be investigated independently and then combined into a complex geometry that yields beneficial results.

In 2000, Nissan Motor Company utilised Ti6Al4V inlet valves in one of their production vehicles with great success, even though literature states that working temperatures inside the engine combustion chamber reaches temperatures exceeding safe working temperature of 350°C. This shows that the alloy is capable of operating under high temperature and high cyclic stress conditions with the correct post production procedures.

The component is also not a complex shape, which is generally the governing reason for employing the investment casting process. For this specific symmetrical geometric shape alternative manufacturing processes would be more viable and more cost effective. The study, however, illustrated that the casting parameters could be individually investigated and the results, where applicable, could then be transferred to more complex engine components.

5.2 Future work

After investigation of the individual cases, it was determined that, in order to improve or verify the relationships for each case, additional numerical simulations must be completed using smaller increments of the relevant parameters.

To verify the soundness of the final design, the simulation must be experimentally reproduced. After this process, the mechanical and microstructural properties must be obtained. The required properties for the valve component must be obtained from industry and the experimental results must be compared.

To obtain components from Ti6Al4V alloy suitable for use in an internal combustion engine at 500°C, additional post processing techniques would need to be investigated such as, HIP and heat treatment of the material.

Radiation view factors and the influence on solidification rate must be further investigated due to effects on complex geometry.

Investigation into centrifugal casting could yield beneficial results as this would potentially remove porosity observed in the stem.

As investment casting is a process specifically for low volume high quality components that would be difficult or impossible to manufacture in any other way due to complexity, thin walls and type of material. Alternative low volume high quality engine components must be investigated in further studies that would be more suited for the investment casting process.

LIST OF FIGURES

Figure 1.1 - Combustion chamber of an internal combustion engine [33].	3
Figure 1.2 - Ti6Al4V phase diagram [100].	5
Figure 1.3 - Investment casting process under gravity [37].	10
Figure 2.1 - Graph illustrating the effect of latent heat of solidification on the final temperature of the casting.	16
Figure 2.2 Investment casting top section through inlet feeders indicating radiation analysis.	19
Figure 2.3 - Discretised space of the domain.	20
Figure 2.4 - FDM investigated space with mesh.	23
Figure 2.5 - Illustrating the difference in meshing in the FEM and FDM space.	25
Figure 3.1 Manufacturing drawing of investigated inlet valve	26
Figure 3.2 - Sectioned valve.	27
Figure 3.3 - Geometrical set-up and illustration of alteration to component angle from 0 to 90°.	33
Figure 3.4 - Alteration of inlet length from 5mm to 23mm.	37
Figure 3.5 - Graph representing distance of porosity from surface of casting head.	38
Figure 3.6 - Geometrical set-up and alteration of inlet geometry diameter for Case 3.	39
Figure 3.7 - Change of porosity with respect to change of diameter of inlet feeder.	40
Figure 3.8 - Temperature distribution at thermocouple (1) for Case 3 from 6mm to 22mm inlet feeder diameter.	41
Figure 3.9 – Cooling curves at thermocouple (2) for Case 3 for 6mm to 22mm inlet feeder diameter.	41
Figure 3.10 – Cooling curve and cooling rates for thermocouple 1 - 14mm inlet feeder diameter.	42
Figure 3.11 - Cooling curve and cooling rates for thermocouple 1 - 22mm inlet feeder diameter.	42
Figure 3.12 - Illustration of the shapes of inlet feeder under investigation.	44
Figure 3.13 – Position of porosity on the surface of the head of the component with respect to inlet feeder shape.	44
Figure 3.14 - Geometrical set-up and alteration of inlet angle for case 5.	46
Figure 3.15 - Effect of change of inlet angle to position of porosity.	46
Figure 3.16 - Geometrical set-up and alteration of inlet angle diameter for case 6.	48
Figure 3.17 - Effect of changing insulation diameter to the position of porosity.	49

Figure 3.18 - Effect of changing insulation diameter to the solidification initiation temperature.	49
Figure 3.19 – Effect of change to initial temperature.	51
Figure 3.20 - Illustration indicating the effect of changing pouring time to the position of porosity with respect to the surface of the component head.	53
Figure 3.21 - Position of porosity with respect to the surface of the component head as mould temperature is increased.....	54
Figure 3.22 - Solidification time as a function of mould temperature.	55
Figure 4.1 - Final design casting tree. Side and top view respectively.....	58
Figure 4.2 - Illustration of porosity observed in the lower half of the casting tree.....	59
Figure 4.3 - Illustration of porosity observed in the upper half of the casting tree.	59
Figure 4.4 - Temperature at the surface of the valve component at the time final part of casting solidifies.....	60
Figure 4.5 - Cooling curves for representative components for the casting tree.	61

LIST OF TABLES

Table 1.1 - Composition of Ti-6Al-4V [31].	4
Table 3.1 - Table used to determine modules of feeder [77].	28
Table 3.2 - Data used to determine diameter and length of downsprue [77].....	29
Table 3.3 - Illustration of localised investigations on the inlet feeder and component.	32
Table 3.4 - Initial and boundary conditions for change of component orientation.	33
Table 3.5 - Initial and geometric conditions for change of inlet length.	36
Table 3.6 - Initial and geometric conditions for change of inlet diameter.	39
Table 3.7 - Initial and geometric conditions for change of inlet feeder shape.	43
Table 3.8 - Initial and geometric conditions for change of inlet angle.	45
Table 3.9 - Initial and geometric conditions for addition and alteration to insulation diameter.	47
Table 3.10 - Initial and geometric conditions for change of initial pouring temperature.....	50
Table 3.11 - Initial and geometric conditions for change of pouring time.	52
Table 3.12 - Initial and geometric conditions for change of mould temperature.....	54
Table 4.1 - Data obtained from individual investigation and used for final design.....	57

REFERENCES

1. Agarwal DP, Ingersoll CE. 1982. Evaluation of various castability patterns by comparison with practical castings. *Journal for Dental Research*, 45: pp. 921--926.
2. Andersson M, Bergman B, Bessing C, Ericson G, Lundquist P, Nilson H. 1989. Clinical results with titanium crowns fabricated with machine duplication and spark erosion. *Acta Odontologica Scandinavica*. 47(5): pp. 279--286.
3. Anglada, E., Mel'Endez, A., Maestro, L. and Domiguez, I. 2013. Adjustment of Numerical Simulation Model to the Investment Casting Process. *Procedia Engineering*, 63 pp. 75--83.
4. Asgar K. 1988. Casting metals in dentistry: past, present, future. *Advanced Research Dental Journal*, 20: pp. 33--43.
5. Asgar K, Arfaei AH. 1985. Castability of crown and bridge alloys. *Journal of Prosthetic Dentistry*, 54(1): pp. 60--63.
6. Au, S. and Wright, P. 1993. "A comparative study of Rapid Prototyping Technology", paper presented at *ASME Winter Conference Vol.66*, New Orleans, November. pp.73-82.
7. Augthun M, Becker L, Kreutzer H, Sahm PR, Scha"fer W, Scha"dlich-Stubenrauch J. 1989. Untersuchungen zur rechnerischen Simulation des Abku"hlungs- und Erstarrungsvorganges an Vollgu"ßkronen. *Deutsche Zahna"rtzliche Zeitschrift* 44: pp. 849--851.
8. Boyer RR. 1996. An overview on the use of titanium in the aerospace industry. *Material Science Engineering: An Introduction*. Vol 213: pp. 103--14.
9. Baran GR. 1983. The metallurgy of Ni-Cr alloys for fixed prosthodontics. *Journal of Prosthetic Dentistry*, 59(5): pp. 639--650.
10. Bergman B, Bessing C, Ericson G, Lundquist P, Nilson H, Andersson M. 1990. A 2-year follow-up study of titanium crowns. *Acta Odontologica Scandinavica*, 48: pp. 113--117.
11. Bessing C, Bergman M. 1992. The castability of unalloyed titanium in three different casting machines. *Swedish Dentistry Journal*, 16: pp. 109—113.
12. Bezzon OL. 1993. Allergic sensitivity to several base metals: A clinical report. *Journal of Prosthetic Dentistry*, 69(3): pp. 243—244.
13. Bonollo, F., Odorizzi, S., 2001. Numerical simulation of foundry process. Servizi Grafici Editoriali, Padova, Italy.
14. Boyer, R. R. 1996. *Material Science Engineering*. A 213(1-2). pp. 103.
15. Brockhurst PJ, McLaverty VG, Kasloff Z. 1983. A castability standard for alloys used in restorative dentistry. *Journal of Operative Dentistry*, 8: pp. 130—139.
16. Buch, A. 1999. *Pure metals properties*. Materials Park, Ohio: ASM International.

17. Campbell, J. 2003. *Castings – The New Metallurgy of Cast Metals*. Burlington, Mass.: Butterworth Heinemann. pp. 113, 127.
18. Callister, W. D., Rethwisch, D.G., 2010. *Materials Science and Engineering*. 8th edition. John Wiley & Sons. Inc. pp. 419--420.
19. Calvert ED. 1981. An investment mould for titanium casting. Bureau of Mines Report of Investigation No. 8541, US Dept. of the Interior: pp. 1--35.
20. Chai TI, Stein RS. 1995. Porosity and accuracy of multi-unit titanium castings. *The Journal of Prosthetic Dentistry*, 73: pp. 534--541.
21. Chung HG, Jean-Louis M, Mori T. 1994. Achieving high success rates in titanium casting using cold mould. *Journal of Dental Research*, 73: Abstract 2451: pp. 408.
22. Compagni R, Faucher RR, Youdelis RA. 1984. Effects of sprue design, casting machine, and heat source on casting porosity. *Journal of Prosthetic Dentistry*, 52(0): pp. 41--45.
23. Coleman RL. 1928. Physical properties of dental materials (gold alloys and accessory materials). *Bureau of Standards Journal of Research*, 1: pp. 867, 908--916, 933--939.
24. Collings, E. 1984. The physical metallurgy of titanium alloys. *American Society for Metals Metals Park, Ohio*. pp. 2.
25. Covington JS, McBride MA, Slagle WF, Disney AL. 1985a. Castability of alloys of base metal and semiprecious metal for dental castings. *Journal of Operative Dentistry*, 10: pp. 93-97.
26. Covington JS, McBride MA, Slagle WF, Disney AL. 1985b. Quantization of nickel and beryllium leakage from base metal casting alloys. *Journal of Prosthetic Dentistry*, 54(1): pp. 127--136.
27. Craig RG. 1993. *Restorative Dental Materials*, 9th edition. C.V. Mosby Co., Chicago, IL: pp. 44--50, 88, 89, 95--140, 169--171, 450--472.
28. Craig, R., Eick, J. and Peyton, F. 1965. Properties of natural waxes used in dentistry. *Journal of Dental Research*, 44 (6), pp. 1308--1316.
29. Donachie MJ. 1982. *Titanium and titanium Alloys: Source Book*. American Society of Metals, Metals Park, OH: pp. 3--19, 33, 289--291.
30. Donachie MJ. 1988. *Titanium: A Technical Guide*. ASM International, Metals Park, OH: pp. 9--28, 105--112, 158--213.
31. Donachie, M. J. 2000. *Titanium*. Materials Park, OH: ASM International.
32. Easwaran, J. 1987. *Advanced casting technology*. ASM International. Metals Park, Ohio.
33. Easy Science For Kids, (2013). *All About Internal Combustion Engines - Easy Science For Kids*. [online] Available at: <http://easyscienceforkids.com/all-about-internal-combustion-engines/> [Accessed 4 Apr. 2014].
34. Eylon, D., Froes, F. and Gardiner, R. 1983. Developments in titanium alloy casting technology. *Journal of Management*, 35 (2), pp. 35--47.

35. Eylon D, Newman JR, Thorne JK. 1990. Titanium and titanium alloy castings. In: ASM Handbook, Vol. 2. ASM International, Metals Park, OH: pp. 634--646, 1813, 1892--1896.
36. Eylon D, Fujishiro S, Postans PJ, Froes FH. 1985. High-temperature titanium alloys – a review. Titanium technology: present status and future trends. Titanium Development Association. pp. 87--93.
37. Espint.com, (2014). *ESP International - Investment Casting*. [online] Available at: <http://www.espint.com/engineering/best-fit-manufacturing-practices/investment-casting.aspx> [Accessed 29 Jun. 2014].
38. Flemings, M. (1974). *Solidification processing*. 1st ed. New York: McGraw-Hill.
39. Froes, F. H. and Eylon, D. 1984. *Titanium net shape technologies*. Warrendale, Pa.: The Society. pp. 155--178.
40. Fused Deposition Modelling for fast, safe plastic models. 1991. Paper presented at *12th Annual Conference on Computer Graphics*, Chicago, April. pp. 326-332.
41. Gouldsen, C., Blake, P. 1998. Investment Casting Using FDM/ABS Rapid Prototype Patterns.
42. Gregory JK. 1994. Fatigue crack propagation in titanium alloys. In: Carpinteri A, editor. *Handbook of fatigue crack propagation in metallic structures*. Elsevier Science BV. pp. 281--322.
43. Herø H, Syverud M, Waarli M. 1993. Mould filling *Materials* 9: pp. 15--18.
44. Hamanaka H, Doi H, Yoneyama T, Okuno O. 1989. Dental casting of titanium and Ni-Ti alloys by a new casting machine. *Journal of Dental Research*, 68: pp. 1529--1533.
45. Hansen PN, Hartmann GC, Sturm JC. 1991. Elimination of shrinkage defects through use of computer simulation. *AFS Transactions*, 99: pp. 477--483.
46. Hero H, Waarli M. 1991. Effect of vacuum and super temperature on mould filling during casting. Scandinavia. *Journal of Dental Research*, 99: pp. 55--59.
47. Hero H, Syverud M, Waarli M. 1993. Mould filling and porosity in castings of titanium. *Journal of Dental Materials*, 9:pp. 15--18.
48. Hirano S, Tesk JA, Argentar H, Gregory TM. 1987. Casting of dental alloys: Mould and alloy temperature effects. *Journal of Dental Materials*, 3: pp. 307--314.
49. Ida K, Togaya T, Tsutsumi S, Takeuchi M. 1982. Effect of magnesia investments in the dental casting of pure titanium or titanium alloys. *Journal of Dental Materials*, 1(1): pp. 8--21.
50. Ingole, D. S., Kuthe, A. M., Thakare, S. B. and Talankar, A. S. 2009. Rapid prototyping-- a technology transfer approach for development of rapid tooling. *Rapid Prototyping Journal*, 15 (4), pp. 280--290.

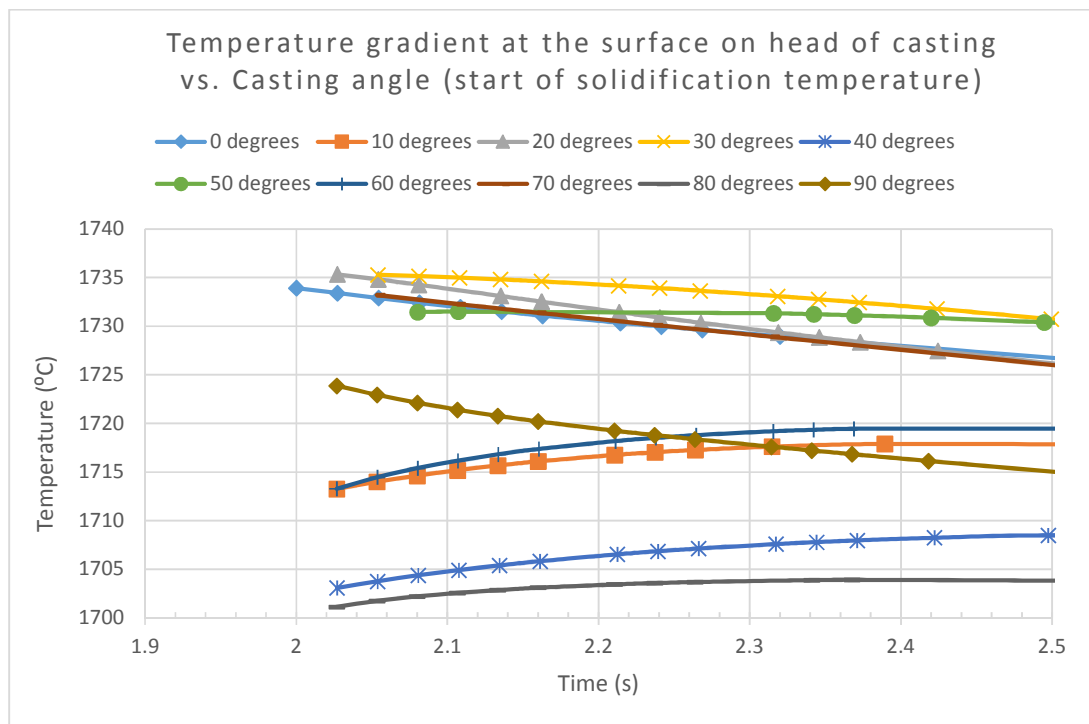
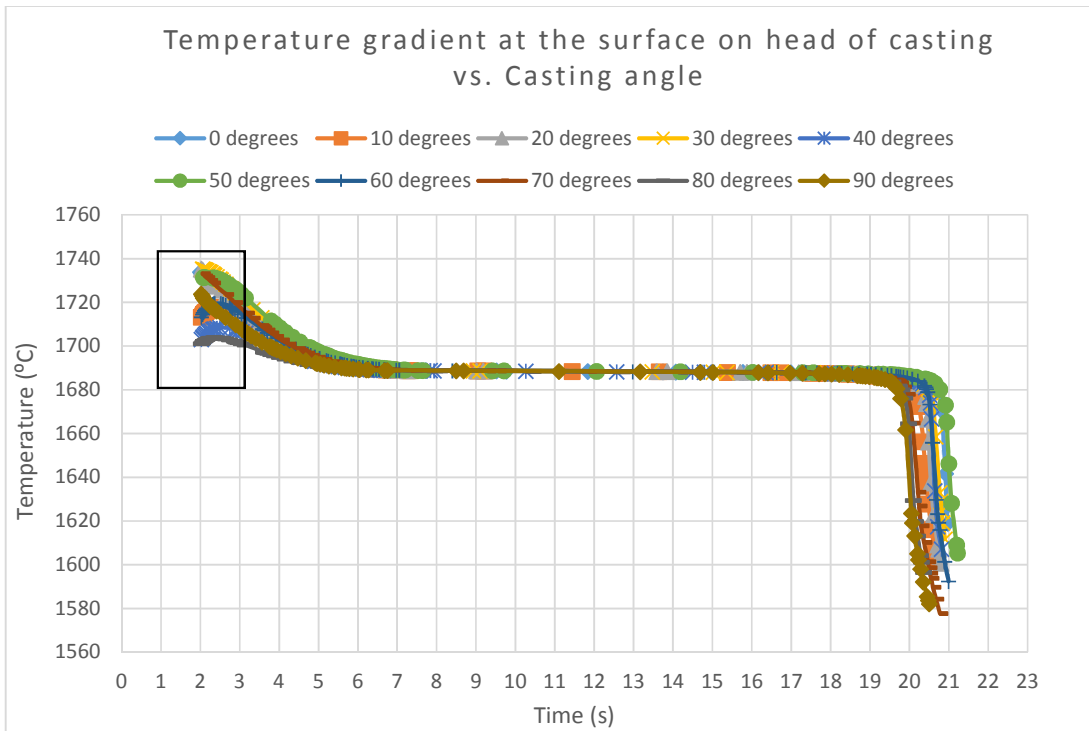
51. Howard WS, Sheldon MN. 1980. Castability of low gold content alloys. *Journal of Dental Research*, 59(5): pp. 824--830.
52. Ida K, Kisaku D, Otani H, Yamaga R. 1969. Studies on fundamental and practical factors in dental casting, Part II. *The Journal of Osaka University Dental School*, 9: pp. 49--61.
53. Jaffee RI, Promisel ME. 1970. The Science, Technology and Application of titanium. Pergamon Press, New York, NY: pp. 5--17, 21--23, 79--84.
54. Jones, S. and Yuan, C. 2003. Advances in shell moulding for investment casting. *Journal of Materials Processing Technology*, 135 (2), pp. 258--265.
55. Kalpakjian, S. and Schmid, S. R. 2008. Manufacturing processes for engineering materials. Upper Saddle River, N.J.: Prentice Hall.
56. Karamangil, M., Avci, A. and Bilal, H. 2008. Investigation of the effect of different carbon film thickness on the exhaust valve. *Heat and Mass Transfer*, 44 (5), pp. 587--598.
57. Kazymyrovych, V. 2009. Very high cycle fatigue of engineering materials: A literature review. Karlstad University.
58. Koch RK, Hoffman JL, Transue ML, Beal RA. 1977. Casting titanium and zirconium in zircon sand moulds. Bureau of Mines Report of Investigation No. 8208, US Dept. of the Interior: pp. 1--44, 126.
59. Kosinar, M. and Kuric, I. Geometric Errors in CNC Machine Tools.
60. Kruth, J.P., Leu, M.C., Nakagawa, T. Progress in Additive Manufacturing and Rapid Prototyping. *Annals of the CIRP*. Vol. 47/2/7998. pp. 425--437.
61. Kuroiwa A, Igarashi Y. 1995. Influence of casting mould size on the titanium casting. *Journal of Dental Research*, 74: Abstract 1834: pp. 241.
62. Leyens, C. and Peters, M. 2003. *Titanium and titanium alloys*. Weinheim: Wiley-VCH.
63. Lewis AJ. 1978. Radiographic evaluation of porosities in removable partial denture castings. *Journal of Prosthetic Dentistry*, 39(3). pp. 278--281.
64. Linefelder KF, Fairhurst CW, Ryge G. 1963. Porosities in dental gold castings: II. Effects of mould temperature, sprue size and dimension of wax pattern. *Journal of American Dental Association*, 67: pp. 816—821.
65. Lynd LE. 1985. Titanium. In: Mineral Facts and Problems. Bureau of Mines Bulletin No. 675, Department of the Interior: pp. 859--879.
66. Magnitskii, O. 1970. Casting properties of titanium alloys.
67. Mason HJ. 1961. Sprue size adjustment in dental castings: Theory of control of heat flow. *Northwest Dentistry*, 40: pp. 127,291—293.
68. Matin KA, Manderson RD. 1984. The influence of sprue design on cobalt chromium alloy casting defects. *Journal of Dentistry*, 12(2): pp. 175--182.

69. McLean J. 1980. Science and Art of Dental Ceramics, Vol. 2. Quintessence Pub. Co., Inc., Chicago, IL: 223--235.
70. Mi J., Harding R. A., Campbell J. 2002. International Journal. *Cast Metals Research*, 14, in press. pp. 10.
71. Mochnacki B., Suchy J. 1995. Numerical Methods in Computations of Foundry Processes. Polish Foundrymen's Technical Associations. Krakow.
72. Miyakawa O, Watanabe K, Okawa S, Nakano S, Honma H, Kobayashi M, Shiokawa N. 1993. Skin holes of titanium casting. *Journal of Dental Materials*, 12(2): pp. 171--181.
73. Myers RE, Pfeiffer KR. 1940. Effect of varying conditions of the time required to cast gold under air pressure. *Journal of American Dental Association*, 27:pp. 530--549.
74. Naylor WP. 1992. Introduction to Metal Ceramic Technology. Quintessence Pub. Co., Inc., Chicago, IL: pp. 68.
75. Oskay, M. and Haney, M. 2010. Computational modeling of titanium structures subjected to thermo-chemo-mechanical environment. *International Journal of Solids and Structures*. Elsevier. pp. 3346.
76. Parr GR, Gardner LK, Toth RW. 1985. Titanium: The mystery metal of implant dentistry: Dental material aspects. *Journal of Prosthetic Dentistry*, 54(3): pp. 410--414.
77. Perzyk, M. (1990). *Materiały do projektowania procesów odlewniczych*. 1st ed. Warszawa: Państwowe Wydawnictwo Naukowe.
78. Phillips RW. 1947. Studies on the density of castings as related to their position in the ring. *Journal of American Dental Association*, pp. 35, 329--342.
79. Polmear IJ. 1981. Light Alloys: Metallurgy of the Light Metals. American Society for Metals, Metals Park, OH: pp. 1--7, 12--14, 163--171, 194--209.
80. Presswood R. 1983. The castability of alloys for small castings. *Journal of Prosthetic Dentistry*, 50(1): pp. 36--39
81. Presten JD, Berger R. 1977. Some laboratory variables affecting ceramic-metal alloys. *Dental Clinics of North America*, 21: pp. 717--728.
82. Regan, T. and Fleck, J. 1986. "Case Studies of Castings Replacing Forgings and Fabrications in a Helicopter Engine, in Advanced Casting Technology", paper presented at Proceedings of an Advanced Casting Technology Conference, Kalamazoo, MI, November. ASM International, pp. 103-110.
83. Reiger MR, Tanquist RA, Vainer S. 1986. The effect of a new sprue design on the castability of a base-metal alloy. *Journal of Prosthetic Dentistry*, 55(6): pp. 686--690.
84. Sach, E., Sima, M., Williams, P., Brancazio, D. and Cornie, J. 1992. Three dimensional printing: Rapid tooling and prototyping directly from a CAD model. *Journal of Engineering for Industry*, 114, pp. 481--488.

85. Sahm PR, Sturm JC. 1986. Solidification in material science in space. Springer-Verlag, Berlin.
86. Sansoz, F. and Ghonem, H. Fatigue Crack Growth Mechanisms in Ti6242 Lamellar Microstructure: Influence of Loading Frequency and temperature.
87. Shanley JJ, Ancowitz SJ, Fenster RK, Pelleu GB. 1981. A comparative study of the centrifugal and vacuum-pressure techniques of casting removable partial denture frameworks. *Journal of Prosthetic Dentistry*, 45(1): pp. 18--23.
88. Shell JS. 1925. Metallography of the precious metals used in dentistry. *Journal of American Dental Association*, 12: pp.794—801.
89. Shridar G, Kutumbarao VV, Sarma DS. 1987. The influence of heat treatment on the structure of a near-a titanium alloy. *Metallurgical and Material Transactions*. pp. 877--891.
90. Stewart KL, Rudd KD, Kuebker WA. 1983. Clinical Removable Partial Prosthodontics. C.V. Mosby Co., St. Louis, MO: pp. 357--358.
91. Sunnerkrantz PA, Syverud M, Hero H. 1990. Effect of casting atmosphere on the quality of Ti-crowns. *Scand. Journal of Dental Research*, 98 pp. 268--272.
92. Suzuki KI, Nishikawa K, Watakabe S. 1996. Mould filling and solidification during centrifugal precision casting of Ti-6Al-4V alloys. *Materials Transactions, Journal of Intelligent Manufacturing*, 37: pp. 1793--1801.
93. Syverud, M. and Hero, H. 1995. Mould filling of Ti castings using investments with different gas permeability. *Dental Materials*, 11 (1), pp. 14--18.
94. Taggart WH. 1907. A new and accurate method of making gold inlays. *Dental Cosmos*, 49(11): pp. 1117--1121.
95. Takahashi J, Kimura H, Lautenschlager EP. 1990. Casting pure titanium into commercial phosphate-bonded SiO₂ investment moulds. *Journal of Dental Research*, 69(12): pp. 1800--1805.
96. Takahashi J, Okazaki M, Kimura H. 1993a. Reaction of titanium with trial phosphate-bonded investment moulds. *Journal of Dental Research*, 72: Abstract 1426: pp. 281.
97. Takahashi J, Zhang JZ, Okazaki M. 1993c. Effect of casting method on castability of pure titanium. *Journal of Dental Materials*, 12(2): pp. 245--252.
98. Taylor, P. 1983. "An illustrated history of lost wax casting", paper presented at 17th Annual BICTA Conference.
99. Terkla LG, Laney WR. 1963. Partial Dentures. C.V. Mosby Co., Saint Louis, MO: pp. 244--249.
100. Udomphol, T. (2007). *Titanium and its alloys*. 1st ed. [ebook] Suranaree University of Technology. Available at: http://www.sut.ac.th/engineering/metal/pdf/Nonferrous/05_Titanium%20and%20titanium%20alloys.pdf [Accessed 26 Jun. 2014].
101. Van Noort R. 1978. Titanium: The implant material of today. *Journal of Material Science* 22. pp. 3801--3811.

102. Vincent PF, Stevens L, Basford KE. 1977. A comparison of the casting ability of precious and nonprecious alloys for porcelain veneering. *Journal of Prosthetic Dentistry*, 37(5): pp. 527--536.
103. Voorwald, H., Coisse, R. and Cioffi, M. 2011. Fatigue Strength of X45CrSi93 stainless steel applied as internal combustion engine valves. *Procedia Engineering*, 10 pp. 1256--1261.
104. Watanabe K, Okawa S, Miyakawa O, Nakano S, Shiokawa N, Kobayashi M. 1991. Molten titanium flow in a mesh cavity by the flow visualization technique. *Journal of Dental Materials*, 10(2): pp. 128--137.
105. Waterman, N. A. and Dickens, P. 1994. Rapid product development in the USA, Europe and Japan. *World Class Design to Manufacture*, 1 (3), pp. 27--36.
106. Waterstrat RM, Giuseppetti AA. 1985. Casting apparatus and investment mould material for metals which melt at very high temperatures. *Journal of Dental Research*, 64: Abstract 1278: pp. 317.
107. Williams DF. 1981. Biocompatibility of clinical Implant Materials, Vol. I. CRC Press, Inc., Boca Raton, FL: pp. 10--44,139--141.
108. Wu, M. et al. 1998. Computer aided prediction and control of shrinkage porosity in titanium dental castings. *Journal of Dental Materials*, 14. pp.321—32.

Appendix A – Temperature Gradient At The Surface Of The Head Of The Casting With Respect To Casting Angle



Appendix B – Temperature Gradient At The Surface Of The Head Of The Casting With Respect To Change Of Inlet Feeder Length

